A NUMERICAL STUDY OF STEADY STATE COOLING IN A RAISED FLOOR DATA CENTER WITH A CEILING PLENUM RETURN

By

JAMIE D. LEVINSON

A thesis submitted to the

School of Graduate Studies

Rutgers, The State University of New Jersey

In partial fulfillment of the requirements

For the degree of

Master of Science

Graduate Program in Mechanical and Aerospace Engineering

Written under the direction of

Yogesh Jaluria

And approved by

_____

_____

_____

New Brunswick, New Jersey

January, 2021

ABSTRACT OF THE THESIS

A NUMERICAL STUDY OF STEADY STATE COOLING IN A RAISED FLOOR DATA CENTER WITH A CEILING PLENUM RETURN

By JAMIE D. LEVINSON

Thesis Director:

Yogesh Jaluria

In this study, the ability of a cooling system to remove heat from a data center is investigated. The governing equations with given boundary conditions are solved numerically using ANSYS Fluent 2020R1 which was validated via comparison with the benchmark problem of natural convection in a square cavity. The number of fans present in each server, the hot aisle width, the ceiling height, and the use of hot aisle containment was varied to determine their influence on how well the data center was cooled. The server racks are modeled as porous media and the temperatures at key location are used to determine various thermal metrics which allows for an investigation of the changes at both the room and rack level.

ACKNOWLEDGEMENTS

I would first like to thank my advisor Dr. Yogesh Jaluria, who has provided me with guidance and support throughout the process of completing this thesis. I would like to thank those who sat on the defense committee for their time and assessing my work. Lastly, I would like to thank my family, who has provided me with endless support and encouragement.

TABLE OF CONTENTS

LIST OF FIGURES

LIST OF TABLES

NOMENCLATURE

A	Area $[m^2]$
$\mathbb{V}$	Volume $[m^3]$
ρ	Density $[kg\ m^{-3}]$
u, v	Velocity $[m\ s^{-1}]$
k	Turbulent kinetic energy $[m^2 s^{-2}]$
P	Pressure $[N\ m^{-2}]$
c_p	Specific heat capacity $[J\ kg^{-1}K^{-1}]$
$\mathrm{C}_2, \mathrm{C}_{1\epsilon}, \mathrm{C}_{3\epsilon}$	Constants
E	Total internal energy per unit mass $[J\ kg^{-1}]$
T	Temperature [K]
$S_h, S_k, S_\epsilon, S_y$	User defined source terms
SHI	Supply Heat Index
RHI	Return Heat Index
RTI	Return Temperature Index
q	Heat flow rate $[W]$
Q	Volumetric flow rate $[m^3 s^{-1}]$
Ra_x	Rayleigh Number
D_H	Hydraulic Diameter $[m]$
U	Area averaged velocity $[m\ s^{-1}]$
C	Inertial resistance factor $[m^{-1}]$

Greek Symbols

μ	Dynamic Viscosity $[kg\ m^{-1}s^{-1}]$

μ_t	Eddy/Turbulent Viscosity $[kg\ m^{-1}s^{-1}]$
ν	Kinematic viscosity $[m^2s^{-1}]$
ς	Short Orifice Correction Coefficient
ϵ	Turbulent Dissipation Rate
ε	Absolute Roughness [m]
τ	Shear Stress $[N\ m^{-2}]$
κ	Thermal conductivity $[W\ m^{-1}K^{-1}]$
κ_t	Turbulent thermal conductivity $[W\ m^{-1}K^{-1}]$
α	Thermal diffusivity$[m^2s^{-1}]$, Permeability $[m^2]$
β	Thermal expansion coefficient $[K^{-1}]$, Beta index
ζ	Loss coefficient
φ	Porosity, Open Area Ratio

Subscripts

f	Fluid
s	Solid
ND	Non-Dimensional
NR	Non-Recoverable
BF	Body force
MBF	Modified Body Force

Operators

⟨a⟩	Volume Average
|a|	Absolute Value
$\bar{a}$	Time Average

CHAPTER 1: INTRODUCTION

1.1 Motivation

Within the last several decades there have been many technological advancements, many of which have necessitated a dramatic increase in the amount of data that can be stored, sent, and processed. Data centers are a network of servers that do just that, but as the amount of information sent to these servers increases so too does amount of heat generated by the servers. Due to the increased amount of heat produced by the servers, the effectiveness of cooling systems has become a growing concern as it becomes more costly and more difficult to ensure that the servers do not overheat.

Just as the amount of information that a data center needs to process has increased, so too have the capabilities of computers. With advances in computers, Computational Fluid Dynamics (CFD) has quickly become a widely implemented tool in the design of modern data centers to reduce hotspots and optimize the layout and design in an attempt to keep data centers cool.

1.2 Previous Work

There are many different parameters that play a role in determining the flow field and heat transfer which occurs inside data centers. Schmidt[1, 2] investigated a steady state, three-dimensional comparison between experimentally and numerically obtained results which indicated that the CFD model using the standard k-ε model had a tendency to exaggerate the hot and cold spots as well as inhibit mixing and thermal dissipation between hot and cold air streams. Much of recent research investigates the effect of the flow through the floor tiles on the rack intake temperatures. Accurately modeling airflow

through the floor tiles is challenging due to the perforations causing the air to exit the tiles as jets. In response to discrepancies of more than 5K at the rack intake and exhaust, Abdelmaksoud investigated various methods of modeling perforated tiles to more accurately model the air entrainment. He recommended a momentum source model to correct for the effects of porosity at places where perforations were present[3]. Joshi and Arghode further developed the model for flow through a perforated tile by accounting for the geometric parameters such as the pore size, pore shape, and perforation pattern[4]. Choi took a closer look at flow and temperature distributions in a server and rack using a software called Thermostat using the LVEL turbulence model. He investigated how interactions between multiple servers as well as varying load conditions affected the thermal profile within a rack and compared simulated results with experimentally obtained values[5, 6]. Various metrics have been developed to determine the efficiency of heat removal in data centers. Sharma developed two metrics called the Supply Heat Index (SHI) and the Return Heat Index (RHI). These indices are used to give a measure of the amount of hot air recirculation from the rack exhausts, hot air infiltration from the hot aisles, and cold air bypass in the cold aisles that occurs within the data center. It was observed that the cold aisle and hot aisle widths as well as the ceiling height had a significant impact on the SHI and RHI[7]. A similar index was developed by Herrlin called the Rack Temperature Index (RTI). Similar to SHI and RHI, RTI is used to quantify the amount of hot air recirculation and cold air bypass that occurs within data centers[8]. Herrlin also developed two Rack Cooling Indices (RCIs), RCI_{HI} and RCI_{LO}, which are used to determine how effectively racks are cooled and maintained within a given temperature range based upon a given set of industry standards[9, 10]. The two

RCIs can be very effective indices to assist in reducing the cost of maintaining the health of the server racks due to over and under cooling. Another metric called the β index was created in order to quantify local rack increase temperature. The authors of [11] claimed that SHI, RHI are largely global metrics and as such are only capable of accurately evaluating issues that occur at a global scale. Problems such as hotspots occur at a local scale and therefore the SHI and RHI may display satisfactory values regardless of the presence of localized hot spots which can result in device failures. Therefore in order to detect problems at a local level, a new metric that is evaluated at the local scale must be used[11].

CHAPTER 2: MODEL AND SETUP

2.1 Physical Model

A 2D raised floor data center is modelled using ANSYS DesignModeler. The base model room dimensions excluding the underfloor supply plenum inlets and drop ceiling plenum return vent has a width of 9.6m and a height of 3m. Server and rack sizes are measured in terms of rack units(U) where 1U corresponds to a height of 44.45mm. The servers used in the model are based on based on 1.5U servers. There are 4 server racks each with a width of 0.9m and a height of 2m allowing it to fit 28 servers each sized at 1.5U. This is the same number of servers which would fit in a 42U rack which is a standard size option which is commonly available. During the simulation, the depth was taken to be 0.6m. Since the model is symmetric, only half of the model is simulated, and a symmetry boundary is imposed in order to reduce the mesh count and computation time. The racks and servers contained within are modelled as a porous media while the perforated tiles and the egg crate return grille which separates the ceiling return plenum

from the room are modelled using a one-dimensional porous jump boundary condition. The exhaust fans in the servers are modelled using a fan boundary which is located inside of the rack and positioned 2.5cm upstream from the rack exhaust. The outlet vent has a width of 0.9m and is located 1.5m above the ceiling egg crate return grille. The cold aisle and perforated tiles are 0.6m wide which is the standard size of perforated tiles with the inlets being located 0.175m below the perforated tiles.

There are several common conventions when designing the layout of a data center. Pitch is the distance from the center of one cold aisle to the center of the next cold aisle. One of these conventions is to have a 7-tile pitch with each cold aisle width having 2 tiles which are each 0.6m, thus the hot aisle has 2 tiles giving it a width of 1.2m. One of many reasons why the width of the hot aisle might vary is that the width of the racks being used can vary or that a higher capacity data center might use 3 tiles in each cold aisle in order to supply the racks with more air.

There is a total of 11 different cases being tested where the number of fans per server, hot aisle width, ceiling height, and use of hot aisle containment are varied. The various case details are provided in Table 2-1.

In every case the solid portion of the porous media is copper. The fluid used in the simulation is air, which is modelled as an incompressible ideal gas due to the importance of buoyancy effects. To use the incompressible ideal gas model, one must specify the molecular weight which is $28.966\frac{\text{kg}}{\text{kgmol}}$, and the operating pressure which is 101325Pa.

The other properties of air are evaluated at the inlet supply temperature which is $288.15\text{K}(15°\text{C})$, therefore the air has a specific heat at constant pressure of $1007\,\frac{\text{J}}{\text{kg}\cdot\text{K}}$, a thermal conductivity of $0.02476\,\frac{\text{W}}{\text{m}\cdot\text{K}}$,and a dynamic viscosity of $1.802 * 10^{-5}\,\frac{\text{kg}}{\text{m}\cdot\text{s}}$.

Case	Ceiling Height [m]	Hot Aisle Width [m]	Fans Per Server	Hot Aisle Containment
1A	3	1.2	2	no
1B			3	
1C (Base Case)			4	
1D			5	
2A		0.9	4	
2B		1.5		
2C		1.8		
3A	2.5	1.2		
3B	2.75			
3C	3.25			
4A	3		3	yes

Table 2-1: Case Specification

The inlets have a fixed velocity and temperature of $1.3\,\frac{\text{m}}{\text{s}}$ and 288.15K respectively while the outlet uses the pressure outlet boundary condition. The walls of the room, vent, and plenum are assumed to be adiabatic while the tops of the racks are treated as coupled walls made of steel and determine the heat transfer by solving a 1D heat equation,

2.2 CFD Modelling

Turbulent flows are modelled using the Reynolds-Averaged Navier-Stokes (RANS) equations

$$\rho\overline{u_j}\frac{\partial\overline{u_i}}{\partial x_j} = \rho\overline{F_i} + \frac{\partial}{\partial x_j}\left[-\overline{P}\delta_{ij} + \mu\left(\frac{\partial\overline{u_i}}{\partial x_j} + \frac{\partial\overline{u_j}}{\partial x_i}\right) - \rho\overline{u'_i u'_j}\right] \quad (1)$$

In this study air is assumed to be an incompressible ideal gas. The realizable k-ϵ model[12] is used to calculate the turbulent kinetic energy(k) and the turbulent dissipation rate(ϵ).

$$\frac{\partial}{\partial t}(\rho k) + \frac{\partial}{\partial x_j}(\rho k u_j) = \frac{\partial}{\partial x_j}\left[\left(\mu + \frac{\mu_t}{\sigma_k}\right) + \frac{\partial k}{\partial x_j}\right] + G_k + G_b - \rho\epsilon - Y_M + S_k \quad (2)$$

$$\frac{\partial}{\partial t}(\rho\epsilon) + \frac{\partial}{\partial x_j}(\rho\epsilon u_j) = \frac{\partial}{\partial x_j}\left[\left(\mu + \frac{\mu_t}{\sigma_\epsilon}\right)\frac{\partial\epsilon}{\partial x_j}\right] + \rho C_1 S\epsilon - \rho C_2 \frac{\epsilon^2}{k + \sqrt{\nu\epsilon}} + C_{1\epsilon}\frac{\epsilon}{k}C_{3\epsilon}G_b + S_\epsilon \quad (3)$$

where $C_1 = \max\left[0.43, \frac{\eta}{\eta+5}\right]$, $\eta = S\frac{k}{\epsilon}$, $S = \sqrt{2S_{ij}S_{ij}}$, and $S_{ij} = \frac{1}{2}\left(\frac{\partial u_j}{\partial x_i} + \frac{\partial u_i}{\partial x_j}\right)$.

The benefit of using the $k-\varepsilon$ type model over the k-ω type model is in its modelling of the bulk flow far away from walls. However, the k-ε type model requires wall functions in order to resolve the flow close to walls. The model used to resolve the near wall flow was the Menter Lechner ε-Equation which is a y+ insensitive and unlike the enhanced wall function does not utilize the turbulent Reynolds number to determine where boundary between the laminar sublayer and the log-law region is located. This is beneficial if there are locations within the center that have low levels of turbulence where the enhanced wall function would be implemented, thus treating those locations as part of a boundary layer. Yet, unlike the standard or non-equilibrium wall functions it allows for

a mesh where the first cell height lies within the viscous sublayer which is important for heat transfer calculations.

Another important equation is the energy transport equation[13]

$$\frac{\partial}{\partial t}(\rho E) + \frac{\partial}{\partial x_i}[u_i(\rho E + P)] = \frac{\partial}{\partial x_i}\left[\kappa_{eff}\frac{\partial T}{\partial x_i} - \left(\sum_q h_q J_{q,i}\right) + \left(\tau_{eff,ij} u_j\right)\right] + S_h \qquad (4)$$

where κ_{eff} is the effective conductivity, S_h is a source term, $J_{q,i}$ is the diffusion flux of species q in direction i, and E is the total internal energy per unit mass. As there is only a single species, there is no diffusion, therefore $J_q = 0$.

$$\kappa_{eff} = \kappa + \kappa_t \qquad (5)$$

$$E = e + \frac{1}{2}u_j u_j = h - \frac{P}{\rho} + \frac{1}{2}u_j u_j \qquad (6)$$

2.3 Thermal Metrics

The return temperature index (RTI) which is introduced by Herrlin and is defined as measure of the energy performance of the air management system[8].

$$RTI = \left[\frac{T_{return} - T_{supply}}{\Delta T_{equip}}\right] 100[\%] \qquad (7)$$

A RTI under 100% implies that there is some amount of air that has bypassed the server rack while a RTI over 100% implies that there is recirculation, and that the server rack is pulling in the heated surrounding air. The target value of RTI is 100% which indicates that only the cold air being supplied from the CRAC is entering the server rack and that none of said air is bypassing the server rack. The RTI is a useful metric for determining how effectively the racks are being cooled.

The supply heat index (SHI) is defined as the ratio of the enthalpy gained between the supply and the rack intake to the total enthalpy gained between the supply and the

rack exhaust. Similarly, the return heat index (RHI) is the ratio of the total enthalpy removed from the data center and extracted by the CRAC units to the total enthalpy gained between the supply and the rack exhaust[7].

$$\mathrm{SHI} = \frac{\delta q_{\text{cold aisle}}}{q_{\text{rack}} + \delta q_{\text{cold aisle}}} = \frac{\sum_i \sum_j \dot{m}_{i,j}^{\text{rack}} c_p \left(T_{\text{intake},i,j}^{\text{rack}} - T_{\text{supply}}\right)}{\sum_i \sum_j \dot{m}_{i,j}^{\text{rack}} c_p \left(T_{\text{exhaust},i,j}^{\text{rack}} - T_{\text{supply}}\right)} \tag{8}$$

$$\mathrm{RHI} = 1 - \mathrm{SHI} = \frac{q_{\text{rack}}}{q_{\text{rack}} + \delta q_{\text{cold aisle}}} = \frac{\sum_k \dot{m}_k^{\text{CRAC}} c_p \left(T_{\text{intake},k}^{\text{CRAC}} - T_{\text{supply}}\right)}{\sum_i \sum_j \dot{m}_{i,j}^{\text{rack}} c_p \left(T_{\text{exhaust},i,j}^{\text{rack}} - T_{\text{supply}}\right)} \tag{9}$$

where δq_{rack} is the total heat dissipation rate from the rack, $\delta q_{\text{cold aisle}}$ is the change in the enthalpy flow rate between the supply and the rack intake, $\dot{m}_{i,j}^{\text{rack}}$, $T_{\text{intake},i,j}^{\text{rack}}$, and $T_{\text{exhaust},i,j}^{\text{rack}}$ are the average rack mass flow rate and the average intake, and exhaust temperatures respectively of i^{th} rack in the j^{th} row of racks. Similarly, $\dot{m}_k^{\text{CRAC}}$ and $T_{\text{intake},k}^{\text{CRAC}}$ are the average CRAC mass flow rate and average intake temperature of the k^{th} CRAC. The change in the enthalpy flow rate between the cold supply air and the rack intake can be attributed to air in the hot aisles mixing with air above the racks or recirculating into the cold aisles whereas the change in enthalpy flow rate between the rack intake and exhaust can be attributed to heat generation by the servers. The SHI and RHI are useful for determining how effectively the heat gained by the air that passes through the rack is advected out of the data center and sent to the CRAC.

The final metric of note is the β Index. The β index can be used to identify where on a rack self-heating and the effects of recirculation occur. This index is defined as

$$\beta = \frac{T_{\text{intake}}^{\text{rack}}(z) - T_{\text{supply}}}{T_{\text{exhaust}}^{\text{rack}} - T_{\text{intake}}^{\text{rack}}} \tag{10}$$

where a value of 0 indicates the absence of recirculation and value greater than 1 is indicative of a self-heating loop that results in local temperatures greater than if the air had just passed through the rack a single time[11].

2.4 Code Validation

In this thesis, all simulations were run using ANSYS Fluent. This code is validated by solving the benchmark problem of natural convection in a square cavity.

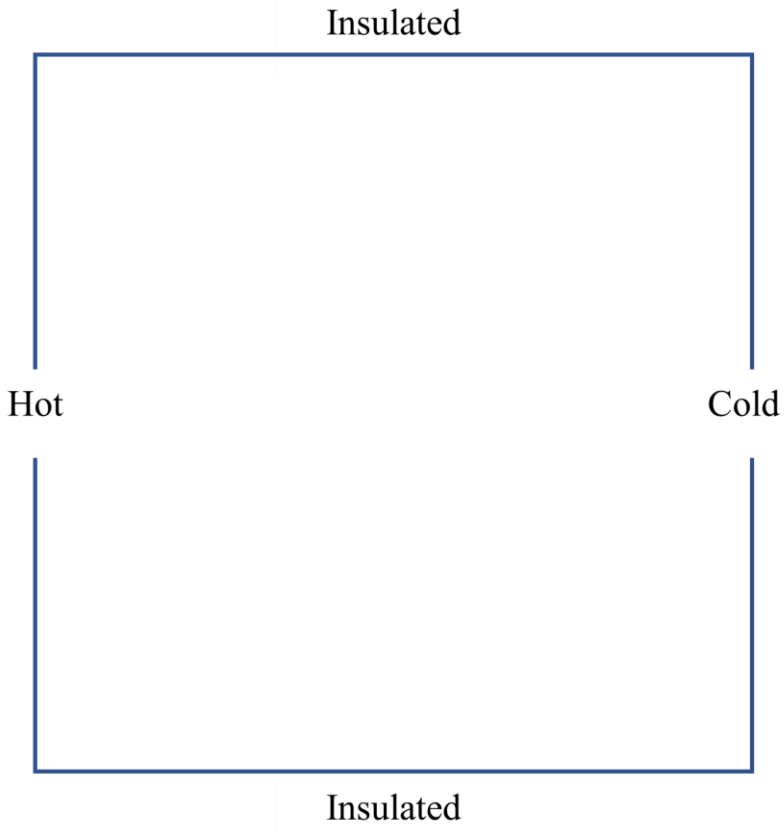

Figure 2-1: Natural convection in a square cavity configuration

$$Ra_x = \frac{g\,\beta}{\alpha\,\nu}(T_s - T_\infty)x^3 \tag{11}$$

where x is the characteristic height, β is the thermal expansion coefficient, g is the magnitude of gravitational acceleration, α is the thermal diffusivity where $\alpha = \frac{\kappa}{\rho\, c_p}$, ν is

the kinematic viscosity where $\nu = \frac{\mu}{\rho}$, T_s is the surface temperature, and T_∞ is the ambient temperature. T_∞ is taken as the temperature at the cold wall, while T_s is the temperature at the hot wall, the temperature of which is determined by the desired value of Ra. The values of the constants were taken as $\kappa = 0.0242 \frac{W}{m \cdot K}$, $c_p = 1006.43 \frac{J}{kg \cdot K}$, $x = 0.1m$, $g = 9.81 \frac{m}{s^2}$, and $T_{Cold} = 288.15K$. A Prandtl number of 0.71 was assumed, therefore the viscosity was determined by $\mu = Pr \frac{\kappa}{c_p}$. The operating temperature was taken to be $T_{op} = \frac{T_{Hot} + T_{Cold}}{2}$, and the thermal expansion coefficient is taken as the inverse of the operating temperature since air is an ideal gas. The density of air was determined by assuming the air was an incompressible ideal gas and evaluating the density at the operating temperature such that $\rho = \frac{P_{op}}{R_{air} T_{op}}$ where R_{air} is the specific gas constant for air and the operating pressure was taken as $P_{op} = 101325Pa$. The following equation was solved for the hot wall temperature at a given Rayleigh Number.

$$\frac{\kappa {R_{air}}^2 \mu}{8 c_p g {P_{op}}^2 x^3} Ra_x = \frac{T_{Hot} - T_{Cold}}{(T_{Hot} + T_{Cold})^3} \tag{12}$$

The values for the maximum horizontal and vertical velocities at the mid-width and mid-height as well as the benchmark solutions are provided in Table 2-2 to Table 2-4. The plot of the Nusselt number at the hot and cold walls as well as the benchmark solution values are provided in figures 2-2 and 2-3. The Nusselt number is defined as

$$Nu = \frac{hL}{\kappa} \tag{13}$$

Where h is the heat transfer coefficient and L is the characteristic length.

Ra	$u_{ND,max}(y_{ND})$	$v_{ND,max}\ (x_{ND})$
10^3	3.634(0.81427)	3.681(0.180219)
10^4	16.179(0.825169)	19.621(0.119068)
10^5	34.744(0.854992)	68.5974(0.065246)
10^6	64.868(0.850306)	220.402(0.038296)

Table 2-2: Maximum horizontal and vertical velocities ($u_{ND,max}$ and $v_{ND,max}$) at the mid-width ($x_{ND} = 0.5$) and mid-height ($y_{ND} = 0.5$) respectively

Ra	Ref [14]	Ref[15]	Ref[16]	Ref [17] FEM	Ref [17] DSC
10^3	3.634(0.813)	3.68(0.817)	3.6493(0.8125)	3.489(0.813)	3.6434(0.8167)
10^4	16.2(0.823)	16.1(0.817)	16.1798(0.8235)	16.122(0.815)	15.967(0.8167)
10^5	34.81(0.855)	34.0(0.857)	34.7741(0.8535)	33.39(0.835)	33.51(0.85)
10^6	65.33(0.851)	65.4(0.875)	64.6912(0.8460)	65.40(0.86)	65.55(0.86)

Table 2-3: Benchmark maximum horizontal velocities ($u_{ND,max}$) at the mid-width ($x_{ND} = 0.5$)

Ra	10^3	10^4	10^5	10^6
Ref[14]	3.679(0.179)	19.51(0.12)	68.22(0.066)	216.75(0.0387)
Ref[18]	–	19.62	68.62	232.97
Ref[19]	3.692	19.63	68.85	221.6
Ref[15]	3.73(0.1827)	19.9(0.1246)	70.0(0.068)	228(0.039)
Ref[16]	3.6962(0.1790)	19.6177(0.1195)	68.6920(0.0665)	220.8331(0.0380)
Ref[17] FEM	3.686(0.188)	19.79(0.12)	70.63(0.072)	227.11(0.040)
Ref[17] DSC	3.686(0.183)	19.98(0.117)	70.81(0.070)	227.24(0.040)

Table 2-4: Benchmark maximum vertical velocities ($v_{ND,max}$) at the mid-height ($y_{ND} = 0.5$)

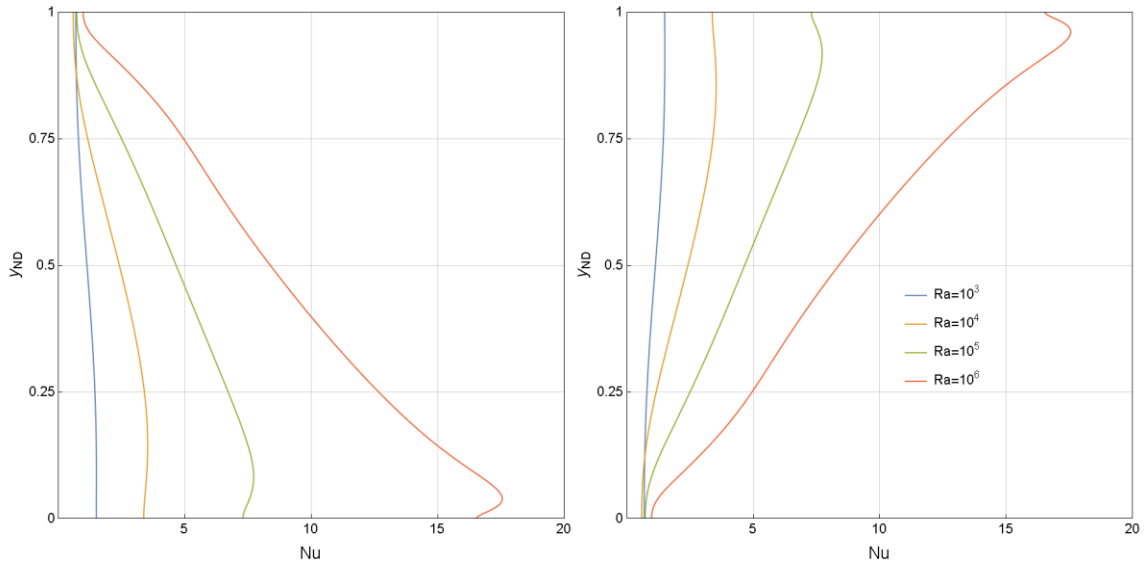

Figure 2-2: Hot(left) and cold(right) wall Nusselt number

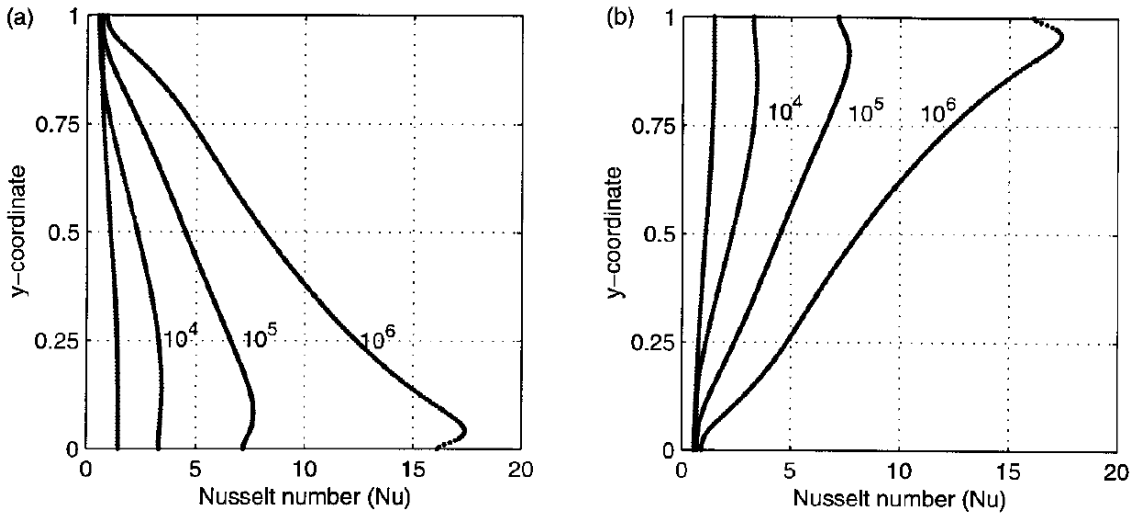

Figure 2-3: Benchmark hot(left) and cold(right) wall Nusselt number[17]

2.5 Perforated Tile Flow Modelling

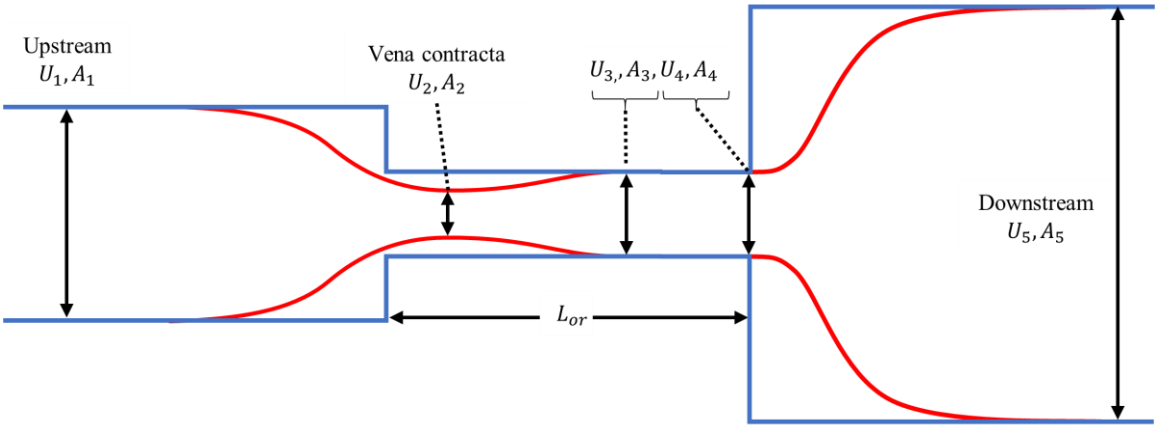

Figure 2-4: Orifice Flow

The loss coefficient is defined as the ratio of the non-recoverable pressure loss between two points to the dynamic pressure at a specified location where the density and velocity is known.

$$\zeta_{a\to b,c} \equiv \frac{\Delta P_{a\to b,NR}}{\frac{1}{2}\rho U_c{}^2} \tag{14}$$

where $\Delta P_{a\to b,NR}$ is the non-recoverable pressure loss as the flow moves from a to b and U_c is the velocity at location c. For the case of turbulent flow, assuming $A_3 = A_4 = A_{or}$ and $U_3 = U_4 = U_{or}$, where A_{or} and U_{or} are the cross-sectional area and mean velocity of the fluid traveling through the orifice, respectively. The open area ratios at the orifice inlet and outlet are $\varphi_{in} = \frac{A_{or}}{A_1}$ and $\varphi_{out} = \frac{A_{or}}{A_5}$ respectively. The loss due to a sudden expansion can be written as

$$\zeta_{4\to 5,or} = (\varphi_{out} - 1)^2 \tag{15}$$

and the loss due to a sudden contraction can be written as

$$\zeta_{1\to 3,or} = \left(\frac{1}{C_c} - 1\right)^2 \tag{16}$$

where C_c is the contraction coefficient which is defined as the ratio of the cross-sectional areas of the jet at the vena-contracta to the cross-sectional area of the orifice. The loss between points 0 and 3 is purely due to frictional effects with the orifice. Since it is unclear exactly at what point the flow reattaches it is assumed that there are frictional losses with the orifice walls for the entire length of the orifice.

$$\zeta_{3\to4,or} = \begin{cases} 0 & L_{or,rel} \leq 0.015 \\ \lambda\, L_{or,rel} & L_{or,rel} > 0.015 \end{cases} \tag{17}$$

where λ is the darcy friction factor and $L_{or,rel} = \frac{L_{or}}{D_H}$. The darcy friction factor is Reynolds number dependent and can be calculated using the Modified Churchill formula[20]

$$\lambda = \left(\left(\frac{64}{Re}\right)^{12} + \frac{1}{\left[\left(0.8687 \ln\left[\frac{1}{\frac{0.883*\ln(Re)^{1.282}}{Re^{1.007}} + 0.27\varepsilon_{rel} - \frac{110}{Re}\varepsilon_{rel}}\right]\right)^{16} + \left(\frac{13269}{Re}\right)^{16}\right]^{\frac{3}{2}}} \right)^{\frac{1}{12}} \tag{18}$$

where $\varepsilon_{rel} = \frac{\varepsilon}{D_H}$ and ε is the absolute surface roughness. The total loss through the orifice can be written as

$$\zeta_{1\to5,or} = \zeta_{1\to3,or} + \zeta_{3\to4,or} + \zeta_{4\to5,or} \tag{19}$$

Equation 19 is only applicable for the case where flow reattachment to the orifice wall is assured. For the case where the length of the orifice is such that the flow may not reattach, the sudden contraction becomes sensitive to flow conditions in the downstream enlargement. As a result, the separated flow at the orifice exit does not agree with the model for a sudden expansion. An orifice model for incompressible flow to account for

the process interactions caused by separation was derived by Dodge based on experimental results[21].

$$\zeta_{\text{corrected},1\to5,\text{or}} = \zeta'\,\zeta_{1\to3,\text{or,Dodge}} + \varsigma\left(\zeta_{1\to3,\text{or,Dodge}}\zeta_{4\to5,\text{or}}\right)^{\frac{1}{2}} + \zeta_{3\to4,\text{or}} + \zeta_{4\to5,\text{or}} \quad (20)$$

where $\zeta_{1\to3,\text{or,Dodge}} = (1-\varphi_{\text{in}})$, ζ' accounts for the inlet edge shape, and ς accounts for the effect of the orifice wall thickness, inlet edge shape, and conditions of flow passage through the orifice[22].

Idelchik made slight modifications to the relationship of a sudden contraction for a sharp edged orifice to better match experimental observations for sharp-edged orifices[22].

$$\zeta_{1\to3,\text{or,Idelchik}} = \zeta'(1-\varphi_{\text{in}})^{\frac{3}{4}} \quad (21)$$

Where $\zeta' = 0.5$ which dictates the maximum value of the loss coefficient of a contraction through a sharp-edged orifice. The value of σ for a thick-edged orifice is[22]

$$\varsigma_{\text{Idelchik}} = \begin{cases} \sqrt{2} & \text{L}_{\text{or,rel}} \le 0.015 \\ \left(2.4-\text{L}_{\text{or,rel}}\right) * 10^{-\left[0.25+\frac{0.535\left(\text{L}_{\text{or,rel}}\right)^8}{0.05+\left(\text{L}_{\text{or,rel}}\right)^7}\right]} & 0.015 < \text{L}_{\text{or,rel}} < 2.4 \\ 0 & \text{L}_{\text{or,rel}} \ge 2.4 \end{cases} \quad (22)$$

Therefore, the loss coefficient of the flow passing through a thick-edged orifice is

$$\zeta_{1\to5,\text{or}} = 0.5(1-\varphi_{\text{in}})^{\frac{3}{4}} + \varsigma_{\text{Idelchik}}(1-\varphi_{\text{in}})^{\frac{3}{8}}(1-\varphi_{\text{out}}) + (1-\varphi_{\text{out}})^2 + \lambda\,\text{L}_{\text{or,rel}} \quad (23)$$

Which can be written in terms of the inlet velocity as

$$\zeta_{1\to5,1} = \frac{\zeta_{1\to5,\text{or}}}{{\varphi_{\text{in}}}^2} \quad (24)$$

It is assumed that a perforated tile can be modelled as a large number of orifices or pores with a combined open area equal to that of a singular larger orifice such that

$\varphi_{tile,in} = \frac{\sum A_p}{A_1}$, $\varphi_{tile,out} = \frac{\sum A_p}{A_5}$, $\varepsilon_{tile,rel} = \frac{\varepsilon_p}{D_p}$, and $Re_{tile} = \frac{U_1 D_{tile}}{\varphi_{tile,in}\nu}$. For the case of a perforated tile made from aluminum that has a surface roughness of 2μm, is 34.8mm thick, has a pore diameter of 12.7mm, an open area ratio of 25%, and is at a temperature of 288.15K at the inlet, and 300K at the vent, the percent of pressure loss attributed to friction is less than 2% for a majority of flow speeds as is show in figure 2-5.

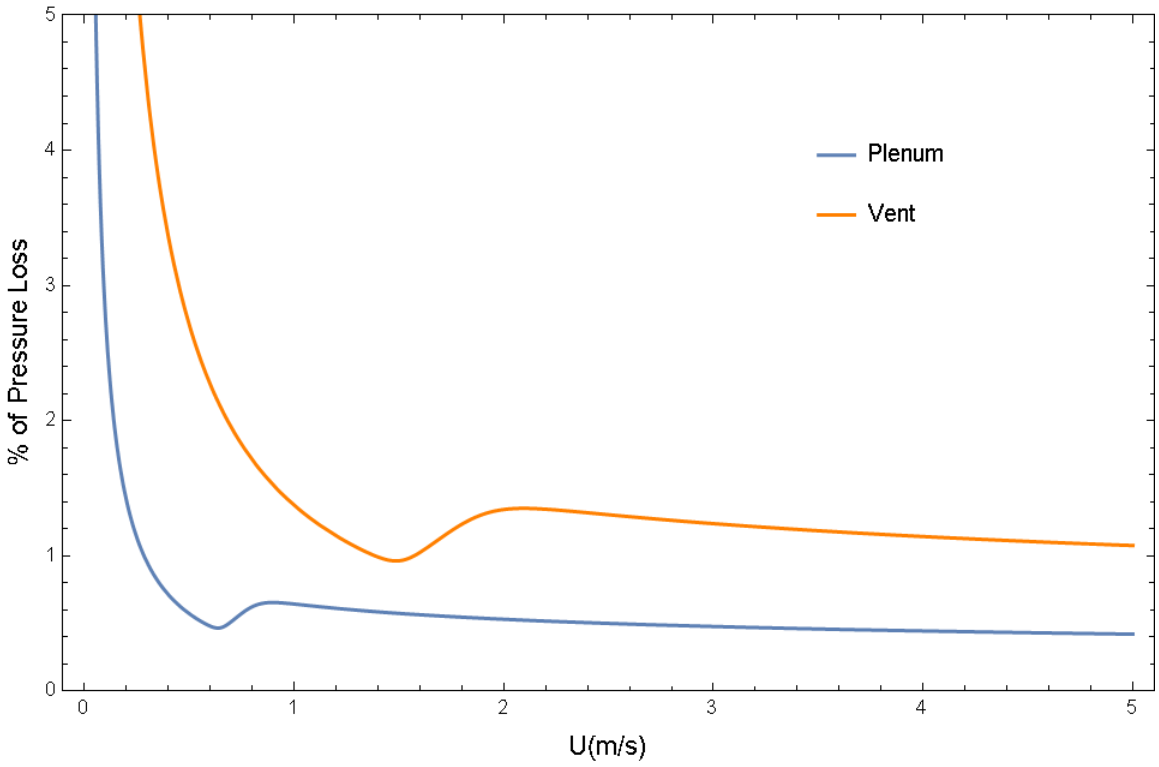

Figure 2-5: Percent of Pressure Loss Through a Perforated Tile Due to Friction

The contributions to the pressure loss due to frictional effects caused by the fluid interacting with the walls is less than 2% of the calculated pressure loss and can be considered negligible thus simplifying the calculation by making it only dependent upon the geometry of the perforated tile.

When using the porous jump model does not preserve the conservation of mass and momentum. To correct for this, the modified body force model developed by Joshi

and Arghode is employed, and for cases where that was not appropriate, the body force model by Abdelmaksoud was utilized. For both models, a Y-momentum source is located above the perforated surfaces to correct for the momentum of the fluid exiting from the perforations. The Y-momentum source is determined by the difference between the Y-momentum flow rate of the fluid approaching the perforated material, and the Y-momentum flow rate of the air through the pores. As it is assumed that flow through each pore can be modelled as orifice flow.

$$U_p = \frac{U_1}{\varphi_{tile}} \tag{25}$$

The magnitude of the Y-momentum source per unit volume used in the Body Force model can be calculated as a function of the density, upstream velocity, and tile porosity[3].

$$S_{y,BF} = \frac{\rho {U_1}^2 \left(\frac{1}{\varphi_{tile}} - 1\right)}{\Delta y_{BF}} \tag{26}$$

U_1 is the average velocity upstream of the perforated tile. The height of the momentum source (Δy_{BF}) is arbitrary and was taken to be 10 cm in all simulations. The modified body force model is more restrictive in its implementation and should only be used if certain criteria are met. These criteria were determined by comparing the modified body force model with a geometrically accurate model[4].

$$\frac{1}{12} < \frac{\Delta y_{MBF}}{W} < \frac{1}{3} \tag{27}$$

$$0.563 < \frac{\varphi_{ref}}{\varphi_{tile}} < 2.25 \tag{28}$$

$$\frac{W}{L_{tile}} > 0.75 \tag{29}$$

where B is the length of the blocked region at the edges of the tile, W is the unblocked side length of the tile, which is assumed to be square, $C_{ref} = 4$ and $\varphi_{ref} = 0.25$. The height of the modified body force is dependent upon the pore diameter and the porosity of the tile

$$\Delta y_{MBF} = C_{ref} D_p \left(\frac{\varphi_{ref}}{\varphi_{tile}}\right)^{0.5} \tag{30}$$

and was determined to be 5 cm based on the properties of the tiles used. The corrected loss coefficient ($\zeta_{1\rightarrow 5,1}{}^{*}$) is dependent on the height of the momentum source height to width ratio, the tile porosity, and the edge blockage.

$$\zeta_{1\rightarrow 5,1}{}^{*} = \zeta_{1\rightarrow 5,1}\left(a\left[\frac{\Delta y_{MBF}}{W}\right] + b\right)\left(\frac{\varphi_{ref}}{\varphi_{tile}}\right)^{n}\left(\frac{W}{L_{tile}}\right)^{m} \tag{31}$$

where $a = -0.351$, $b = 1.214$,$n = -0.138$, and $m = 0.287$. The excess momentum is determined only as a function of the loss coefficient; therefore, the magnitude of the momentum source per unit volume can be determined as a function of the loss coefficient, density, pore diameter, porosity, and the upstream velocity.

$$S_{y,MBF} = \frac{\rho {U_1}^2\left[\left(\zeta_{1\rightarrow 5,1} + 1\right)^{0.5} - 1\right]}{\Delta y_{MBF}} \tag{32}$$

2.6 Server Modelling

The server which was used was a 1.5U server from the open compute project. The average server produces approximately 250W of heat. A 42U rack can fit 28 of these servers therefore each rack produces approximately 7 kW of heat. Modelling a geometrically accurate server as well as the electronic components contained within for every single server present in the rack would require a very fine mesh as well as a tremendous amount of time. Therefore, in order to simplify the model, each rack is

treated as a porous media with a heat source. The porous media has a porosity of 35% as was assumed by Nada et al[23].

2.6.1 Porous Media Modelling

When modelling porous media, the volume is split into its solid and fluid components such that

$$\mathbb{V}_b = \mathbb{V}_s + \mathbb{V}_f \tag{33}$$

Where $\mathbb{V}_b$, $\mathbb{V}_s$, and $\mathbb{V}_f$ are the bulk, solid, and fluid volumes, respectively. To determine the properties in the fluid volume one must define the porosity of the material.

$$\varphi = \frac{\mathbb{V}_f}{\mathbb{V}_b} \tag{34}$$

Darcy's Law calculates the pressure loss across porous media[24]

$$\frac{\partial \langle P \rangle^f}{\partial x} = -\frac{\mu_f}{\alpha}\langle u_i \rangle \tag{35}$$

where α is the permeability. Darcy's law is only valid for the case of laminar flow where the effects of inertial resistance is negligible. For the case of turbulent flow, one uses the Forchheimer equation which adds to Darcy's Law by including a term to account for inertial losses[24]

$$\frac{\partial \langle P \rangle^f}{\partial x} = -\frac{\mu_f}{\alpha}\langle u_i \rangle - \frac{1}{2} C \rho_f |\langle u_i \rangle| \langle u_i \rangle \tag{36}$$

where C is the inertial resistance factor.

The equations for mass and momentum conservation used in ANSYS Fluent that are used to determine the behavior of flow in porous media, can be written using the physical velocity[24].

$$\frac{\partial (\varphi \rho_f)}{\partial t} + \nabla \cdot \left(\varphi \rho_f \langle \vec{u} \rangle^f \right) = 0 \tag{37}$$

$$\frac{\partial\left(\varphi\rho_f\langle\vec{u}\rangle^f\right)}{\partial t}+\nabla\cdot\left(\varphi\rho_f\langle\vec{u}\rangle^f\langle\vec{u}\rangle^f\right)=-\nabla\left(\varphi\langle P_f\rangle^f\right)+\nabla\cdot\left(\varphi\langle\bar{\bar{\tau}}_f\rangle^f\right)+\varphi\rho_f\vec{g}$$
$$-\left(\frac{\varphi^2\mu}{\alpha}\langle\vec{u}\rangle^f+\frac{1}{2}C\varphi^3\rho_f\left|\langle\vec{u}\rangle^f\right|\langle\vec{u}\rangle^f\right) \quad (38)$$

ANSYS fluent solves the standard energy equation in porous media regions. The only change are modifications made to the conduction flux and the transient terms[24].

$$\frac{\partial}{\partial t}(\varphi\rho_f E_f+(1-\varphi)\rho_s E_s)+\nabla\cdot\left(\vec{u}(\rho_f E_f+P)\right)=S_f{}^h$$
$$+\nabla\cdot\left[\kappa_{eff}\nabla T-\left(\sum_q h_q J_q\right)+(\bar{\bar{\tau}}\cdot\vec{u})\right] \quad (39)$$

where $S_f{}^h$ is a fluid enthalpy source term, E_f is the total fluid energy, and E_s is the total solid medium energy. The shear stress$(\bar{\bar{\tau}})$ in the porous region uses an effective viscosity(μ_{eff}) which is determined by the relative viscosity(μ_{rel}) in order to account for the effect of the porous medium[24].

$$\mu_{eff}=\mu_{rel}\mu_{eff} \quad (40)$$

Since the servers are not a true porous media it is assumed that $\mu_{rel}=1$. The porous media is assumed to be in thermal equilibrium; therefore, the porous media uses an effective conductivity[24].

$$\kappa_{eff}=\varphi\kappa_f+(1-\varphi)\kappa_s \quad (41)$$

2.6.2 Determining Resistance Coefficients

The permeability (α) and inertial resistance factor (C) can be obtained by determining the system resistance curve of the servers in the rack. A system resistance curve can be used to determine the relationship between the pressure drop and the volumetric flow rate within a system.

Volumetric Flow Rate (m^3/s)	Pressure (Pa)
0.0	0.0
0.00472	1.09734
0.01605	8.13164
0.02832	22.30076
0.03776	37.66351
0.04719	57.10411

Table 2-5: Server System Resistance Curve Data [25]

The resistance curve was determined to be

$$\Delta P_{static} = B_1 Q_{server} + B_2 {Q_{server}}^2 \quad (42)$$

where $B_1 = 147.221$ and $B_2 = 22.60753$, with a R^2 value of 0.9999997. The pressure loss in terms of the superficial velocity is

$$\Delta P_{static} = B_3 U_{server,superficial} + B_4 {U_{server,superficial}}^2 \quad (43)$$

where $B_3 = 4.66395$ and $B_4 = 22.60753$. The superficial velocity is assumed as measurements are not taken between components and the velocity between the components will be greater than that downstream. The measurements used to obtain the experimental data were taken at $297.15K$ which was used to determine the fluid properties.

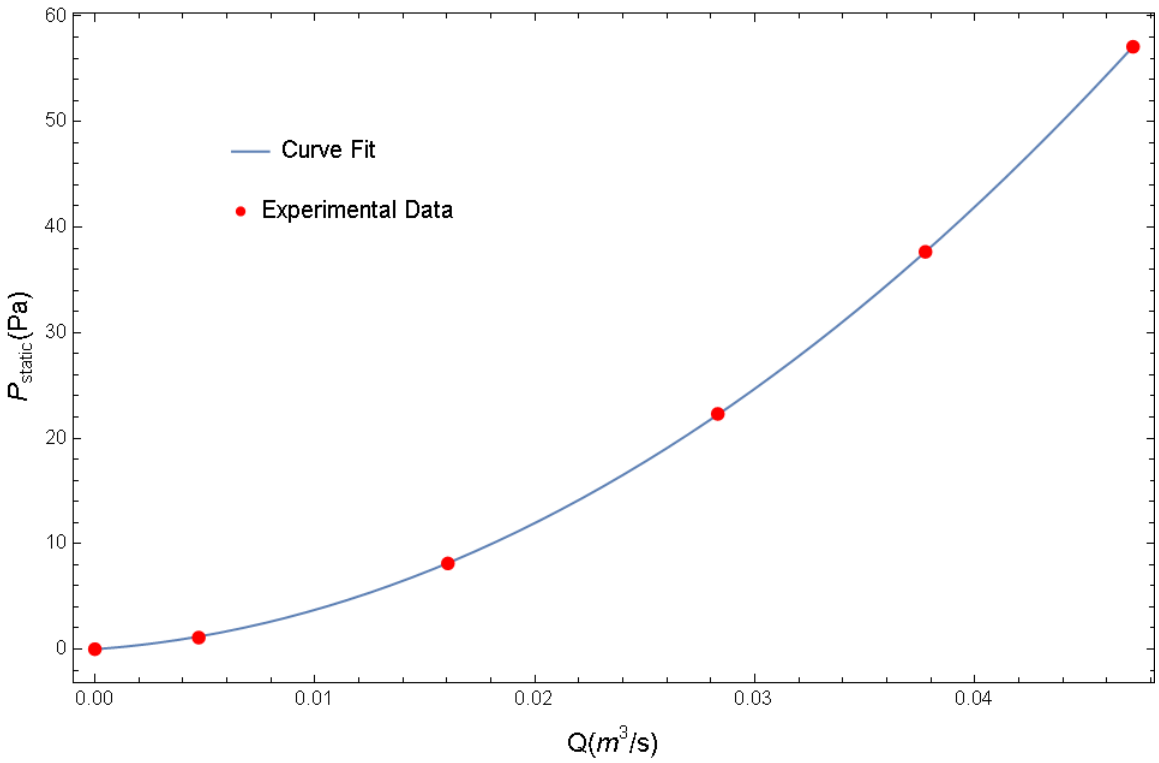

Figure 2-6: Server System Resistance Curve

By using the system resistance curve, the permeability and inertial resistance factor were determined to be $2.33323 * 10^{-6}$ m^2 and 64.07376 m^{-1} respectively. However, a server rack contains more than a single server, therefore an equivalent permeability and equivalent inertial resistance factor are determined to accommodate for the presence of multiple servers and multiple impermeable walls within a single porous block. The equivalent viscous resistance can be calculated by calculated an equivalent resistance of a flow moving through multiple parallel channels.

$$\Delta P_{rack} = \Delta P_{N\ servers} \tag{44}$$

$$U_{rack} = U_{server} \frac{N_{server} * A_{server}}{A_{rack}} \tag{45}$$

Since the primary method of heat transfer in the servers is advection, it is imperative to ensure that the mass flow rate accurately reflects that of an actual server rack. This is

accomplished by making the loss coefficients dependent upon the total area of the rack which is taken up by the servers which are not obstructed. It should also be noted that for the same mass flow rate at the inlet and the same resistance coefficients, for either the physical or superficial velocity formulation one should obtain the same pressure drop across the porous media zone[24]. Therefore, the pressure loss through the rack at a given flow rate should accurately reflect the pressure loss through the individual servers.

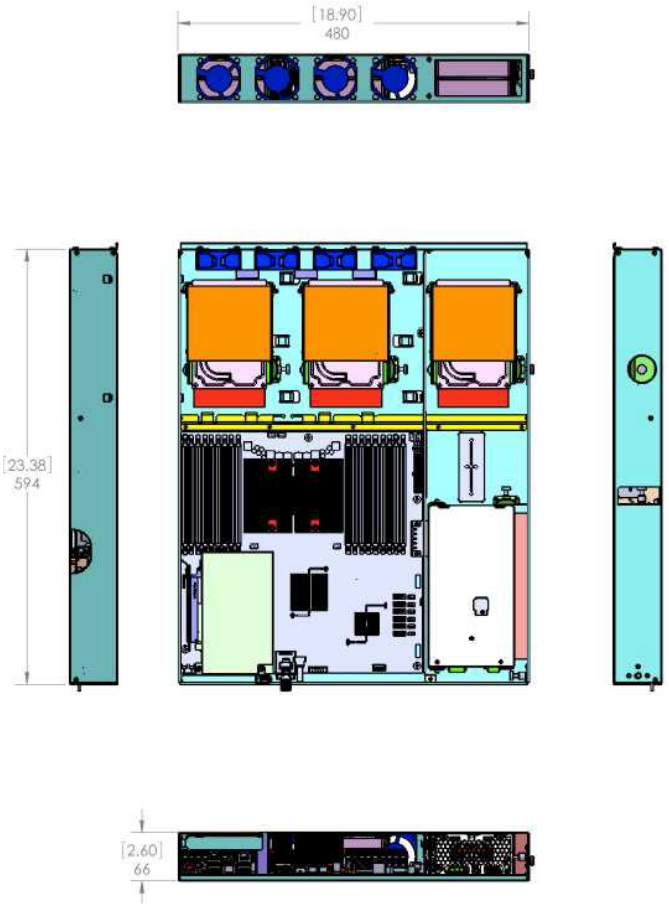

Figure 2-7: Server chassis dimensions in [inches] and mm[26]

The viscous resistance of the entire server rack can be obtained by using the viscous resistance formulation obtained from Poiseuille's law which states that the resistance is

equal to ratio of the pressure drop to the volumetric flow rate for a laminar, incompressible flow for a fluid with constant density.

$$R = \frac{\Delta P}{Q} \tag{46}$$

By relating this to the Darcy equation, the viscous resistance is expressed as

$$R_{viscous} = \frac{\mu_f \Delta x}{\alpha A_c} \tag{47}$$

where Δx is the pathlength that the fluid travels through the porous media and A_c is the cross-sectional area. Since the permeability is solely dependent upon geometric factors it will have the same value in both the laminar and turbulent regime.

An equivalent inertial resistance factor can be obtained using the method of equivalent resistance under the assumptions of constant density within the rack and negligible viscous resistance.

$$R_{inertial} = \frac{C \rho_f Q}{2 {A_c}^2} \tag{48}$$

Thus, by calculating the viscous and inertial resistance and scaling these values based on the length of the server rack used in the simulation such that an equivalent pressure loss is obtained, one can determine the equivalent permeability and inertial resistance for the server rack.

$$\alpha_{rack} = \left(\frac{N_{server} A_{server}}{A_{rack}}\right)\left(\frac{\Delta x_{rack}}{\Delta x_{server}}\right)\alpha_{server} \tag{49}$$

$$C_{rack} = \left(\frac{A_{rack}}{N_{server} A_{server}}\right)^2 \left(\frac{\Delta x_{server}}{\Delta x_{rack}}\right) C_{server} \tag{50}$$

The equivalent permeability and inertial resistance factor for the server rack as a singular porous block are $2.54063 * 10^{-6}$ m^2 and 79.604 m^{-1} respectively. It should be noted

that the pathlength of the flow through the rack used to obtain these values was 0.875m as the fan boundary cannot be placed at the interface of the porous and non-porous domains.

2.6.3 Fan Modelling

To model the effects of a fan in a 2D simulation in Fluent, all that required is a fan curve. A fan curve describes the relationship between the volumetric flow rate and the pressure difference across the fan. The fan which is used as the basis for the fan in the simulation is the Sanace 109R0612P4J06. The dimensions of this fan are 60 mm x 60 mm x 25.4 mm. A fan curve modeled as a third order polynomial was fit to the data from Table 2-7.

Volumetric Flow Rate $(\text{m}^3/\text{s}) * 10^{-2}$	Pressure (Pa)
0.0	141.98067
0.38228	99.13738
0.54746	76.71938
0.66545	69.24671
0.88726	67.25400
1.09964	59.28316
1.33089	41.34876
1.54799	16.93805
1.70373	1.99271

Table 2-6: Single fan pressure curve data[27]

$$\Delta P_{static} = 141.981 - 17889.456Q + 1551420.262Q^2 - 5.818 * 10^7 Q^3 \qquad (51)$$

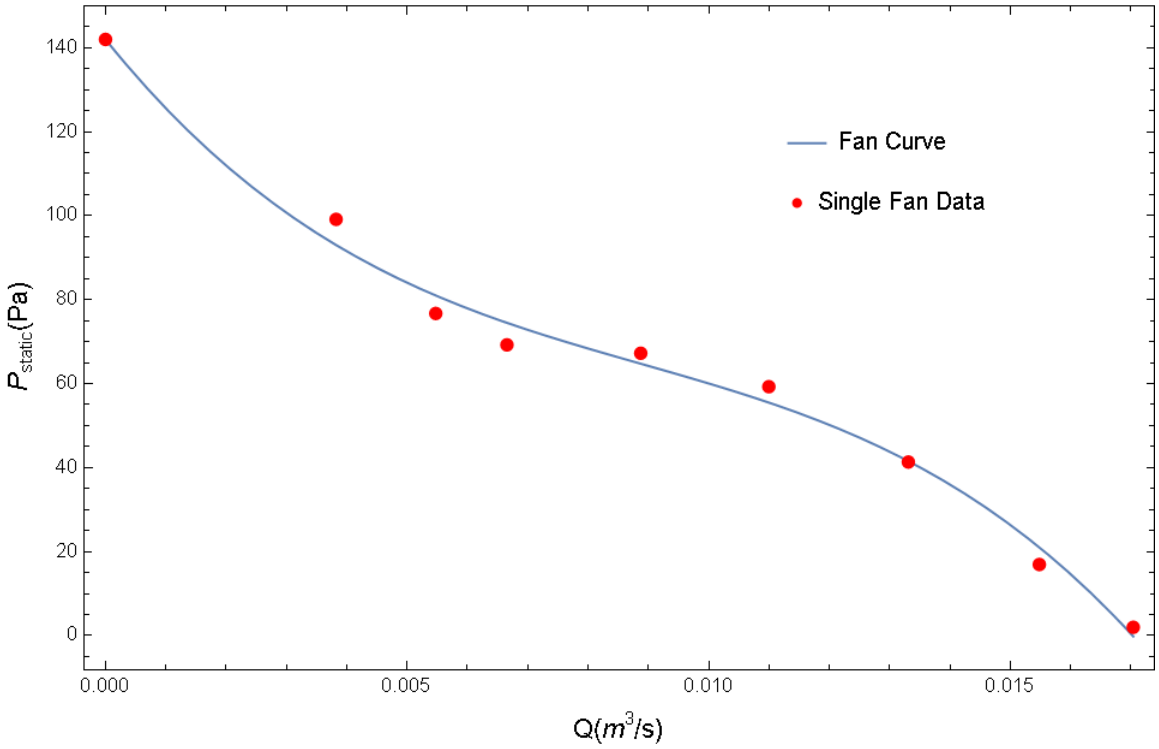

Figure 2-8: Single Fan Curve

with an R^2 value of 0.996. When modelling the fans which are used for the entire rack, an equivalent fan curve for multiple identical fans in parallel can be obtained by using the following relations.

$$\Delta P_{eq\ fan} = \Delta P_{single\ fan} \tag{52}$$

$$Q_{eq\ fan} = U_{eq\ fan} A_{eq\ fan} = \sum_{n=1}^{N_{fan}} Q_{single\ fan} \tag{53}$$

where N_{fan} is the total number of fans in the server rack. In the simulations the number of fans which are being used are 2, 3, 4, and 5 fans per server or 56, 84, 112, and 140 fans per rack, which are being modelled as a single equivalent fan placed on the rear of the rack. The volumetric flow rate for the equivalent fan used in the rack, assuming all fans are identical is equal to the volumetric flow rate through the rack.

$$Q_{eq\ fan} = U_{rack} A_{rack} \tag{54}$$

The equivalent fan curve in terms of velocity through the rack for the entire server rack is

$$\Delta P_{static,56\ fans} = 141.981 - 383.363U_{rack} + 712.459U_{rack}^{2} - 572.493U_{rack}^{3} \quad (55)$$

$$\Delta P_{static,84\ fans} = 141.981 - 255.576U_{rack} + 316.649U_{rack}^{2} - 169.628U_{rack}^{3} \quad (56)$$

$$\Delta P_{static,112\ fans} = 141.981 - 191.682U_{rack} + 178.115U_{rack}^{2} - 71.562U_{rack}^{3} \quad (57)$$

$$\Delta P_{static,140\ fans} = 141.981 - 153.345U_{rack} + 113.994U_{rack}^{2} - 36.640U_{rack}^{3} \quad (58)$$

The equivalent fan is modelled at the rear end of the server at the exhaust and is used to pull air in from the cold aisle and out into the hot aisle.

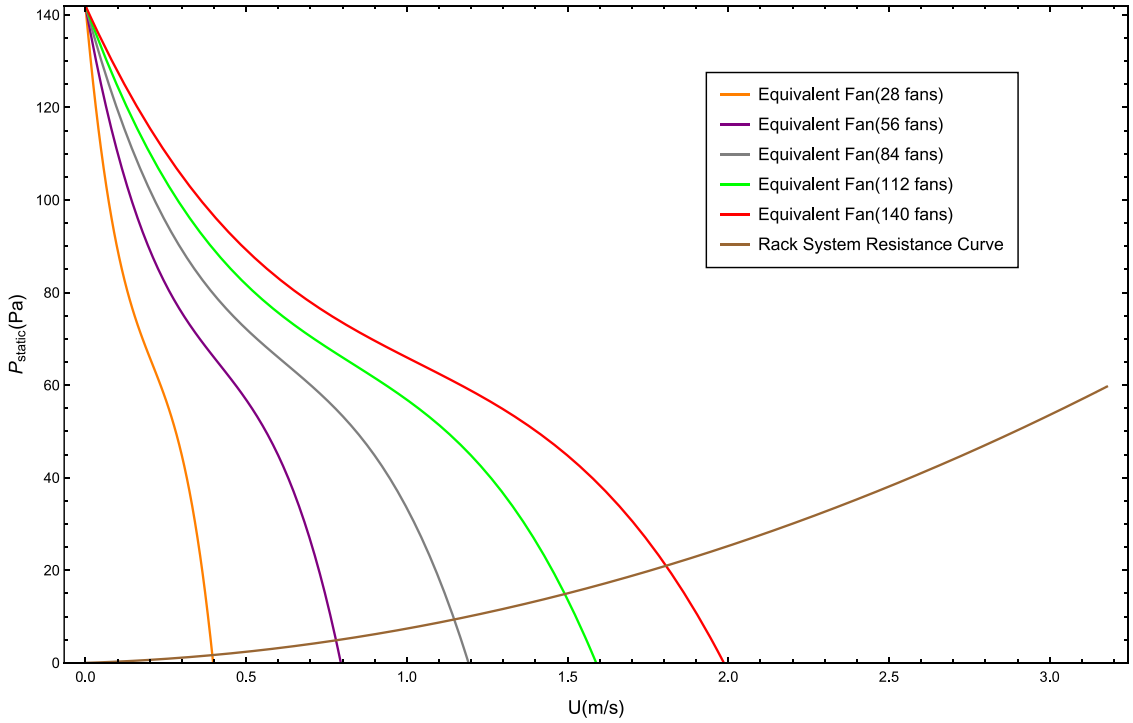

Figure 2-9: Fan and system resistance curves in terms of physical velocity

One can predict the operating velocity through the rack by locating the operating point which is located at the intersection of the fan curve and the system resistance curve.

2.7 Grid Dependency

The simulations are performed using ANSYS 2020R1 (Fluent). A mesh convergence study has been carried out for case 1C to ensure that results are mesh independent. The mesh convergence test was run using the coupled, pseudo-transient solver for the case

with a ceiling height of 4m as this has the largest domain. The solution was considered converged when the globally scaled continuity, x-velocity, y-velocity, energy, k, and epsilon residuals dropped below 10^{-6}. In addition to using residuals to determine convergence, average temperatures of the rack intakes, rack exhausts, vent outlet, and at the fluid above the racks and adjacent to the cold aisles were monitored as well as the mass flow rate through the racks. With regards to the monitored values, the solution was considered converged. The residual of the monitored quantities is

$$\mathrm{Res(Np)} = \frac{|\mathrm{m(n)} - \mathrm{m(n - Np)}|}{\mathrm{m(n)}} \tag{59}$$

where n is the current iteration/time step number, $\mathrm{m(n)}$ is the report value at the n^{th} iteration/time step, and Np is the number of previous iterations/time steps to consider. The monitored quantities are considered converged when

$$\mathrm{Max[Res(1), \dots, Res(Np)]} < \text{Stop Criterion} \tag{60}$$

The stop criterion was set to 10^{-6} over 100 iterations. Mesh convergence was determined when variations in SHI, RHI, and RTI were less than 0.1%. The mesh for cases 1A, 1B, 1C, and 1D are given in figure 2-10.

Elements	183807	326768	510575
RHI (% difference)	0.7422	$0.7420(-0.0285\%)$	$0.7417(-0.0344\%)$
SHI (% difference)	0.2641	$0.2651(0.3951\%)$	$0.2652(0.0215\%)$
Rack 1 RTI (% difference)	128.497	$128.712(0.1679\%)$	$128.664(-0.0375\%)$
Rack 2 RTI (% difference)	129.471	$129.566(0.0732\%)$	$129.565(-0.0008\%)$

Table 2-7: Mesh convergence test

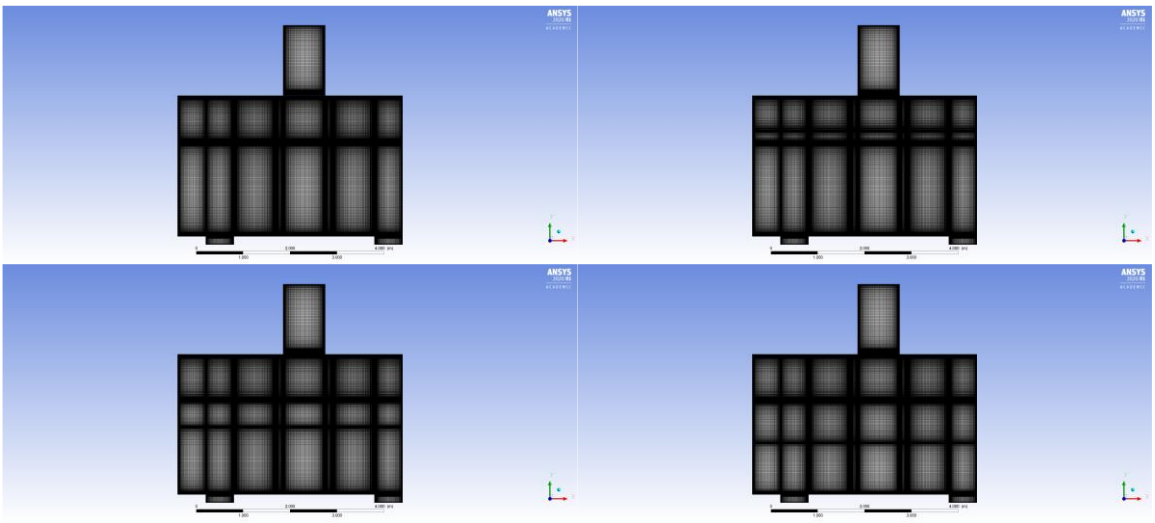

Figure 2-10: Mesh for cases 1A (top left), 1B (top right), 1C (bottom left), and 1D (bottom right)

CHAPTER 3: RESULTS AND DISCUSSION

3.1 Fans Per Server

The number of fans located within each server is 2 to 4 fans per server with 28 servers per rack. By increasing the number of fans in each server the maximum possible volumetric flow rate will increase multiplicatively proportional to the number of fans present. The fans will operate by accelerating the flow to overcome the pressure loss incurred within the servers. By doing so, the volumetric flow rate through the server racks is increased and the effects of this can be observed.

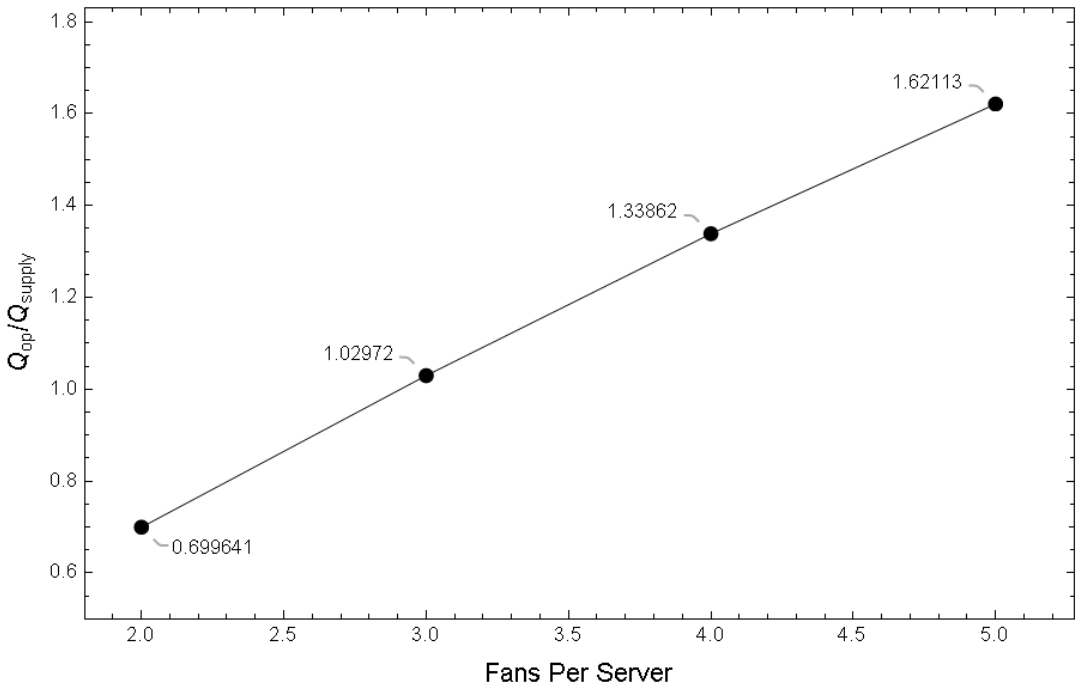

Figure 3-1: Variation of volumetric flow rate ratio with fans per server

Not all fans are the same and have varying sizes and fan curves, and the variation in the temperature and density of the air is unknown beforehand, therefore when determining the effect of the number of fans on the various indices, the effect of the ratio of the operating volumetric flow rate to the supply volumetric flow rate shall be observed rather than the specific number of fans. The relationship between the number of fans per server and the volumetric flow rate ratio is shown in figure 3-1. The error of the sum of the SHI and RHI for cases 1A, 1B, and 1C are all under 2% as is shown in figure 3-2.

As is seen in figure 3-5, when the operating volumetric flow rate is equal to or less than the supply volumetric flow rate that the SHI and RHI are approximately 0 and 1, respectively and increases very gradually up to the point where the volumetric flow rate ratio is unity. This is a result of the temperature at the rack intake being approximately the same as the temperature of the supply air for cases where all or nearly all air that

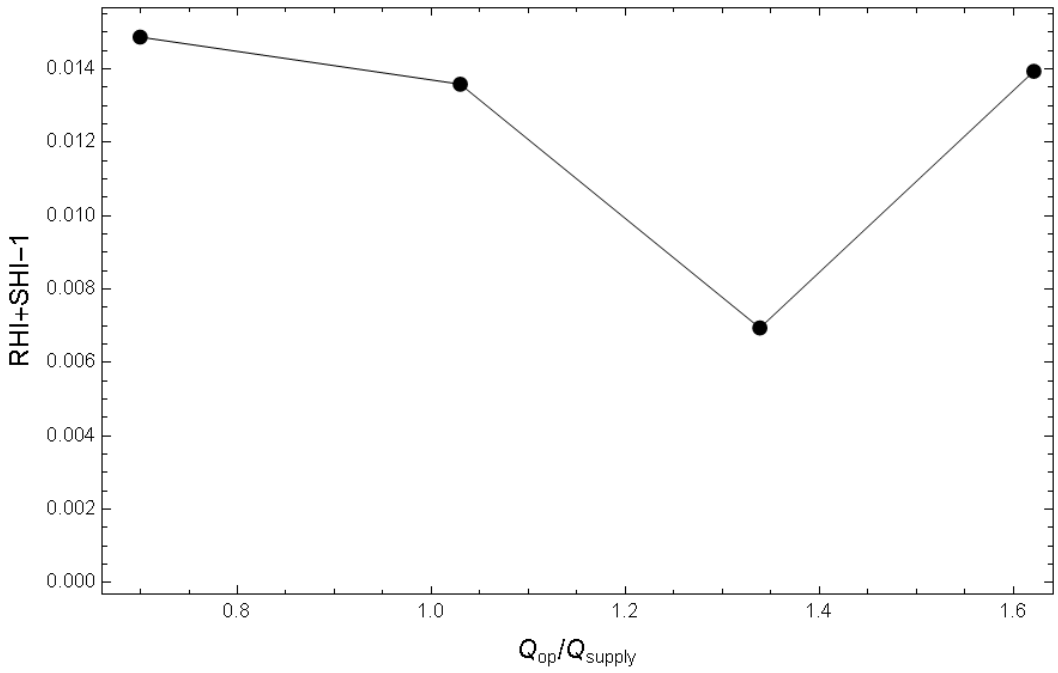

Figure 3-2: Variation of error of sum of SHI and RHI with volumetric flow rate ratio

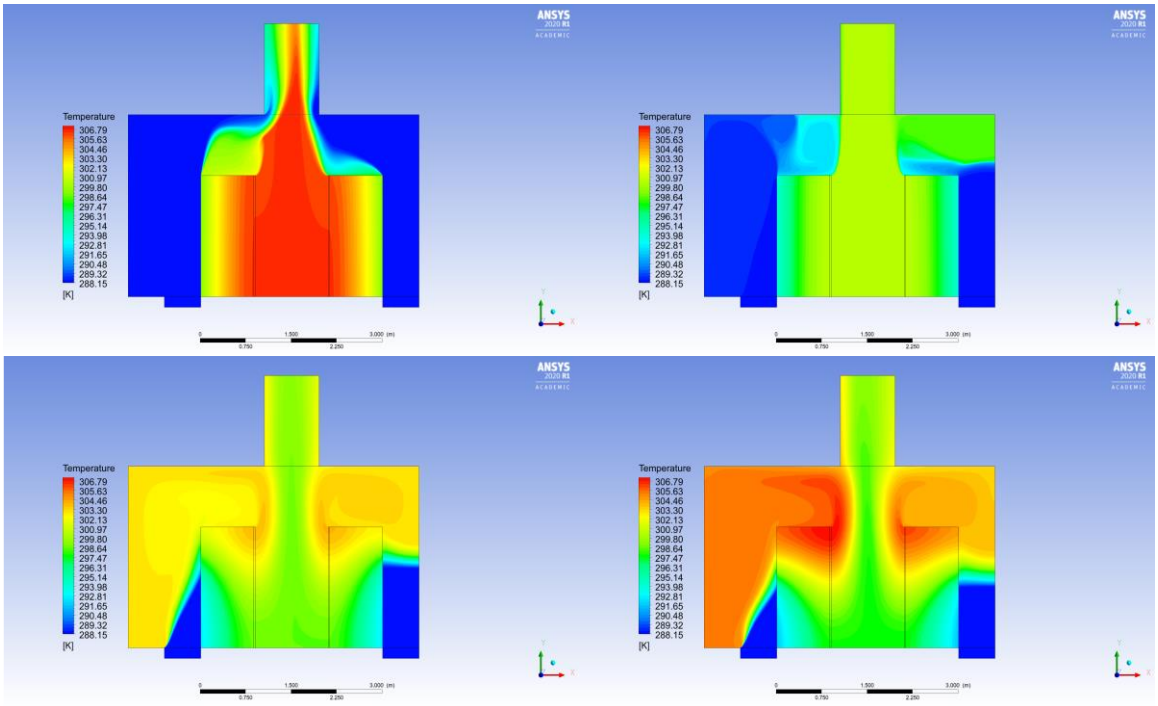

Figure 3-3: 1A (top left), 1B (top right), 1C (bottom left), and 1D (bottom right) temperature contours

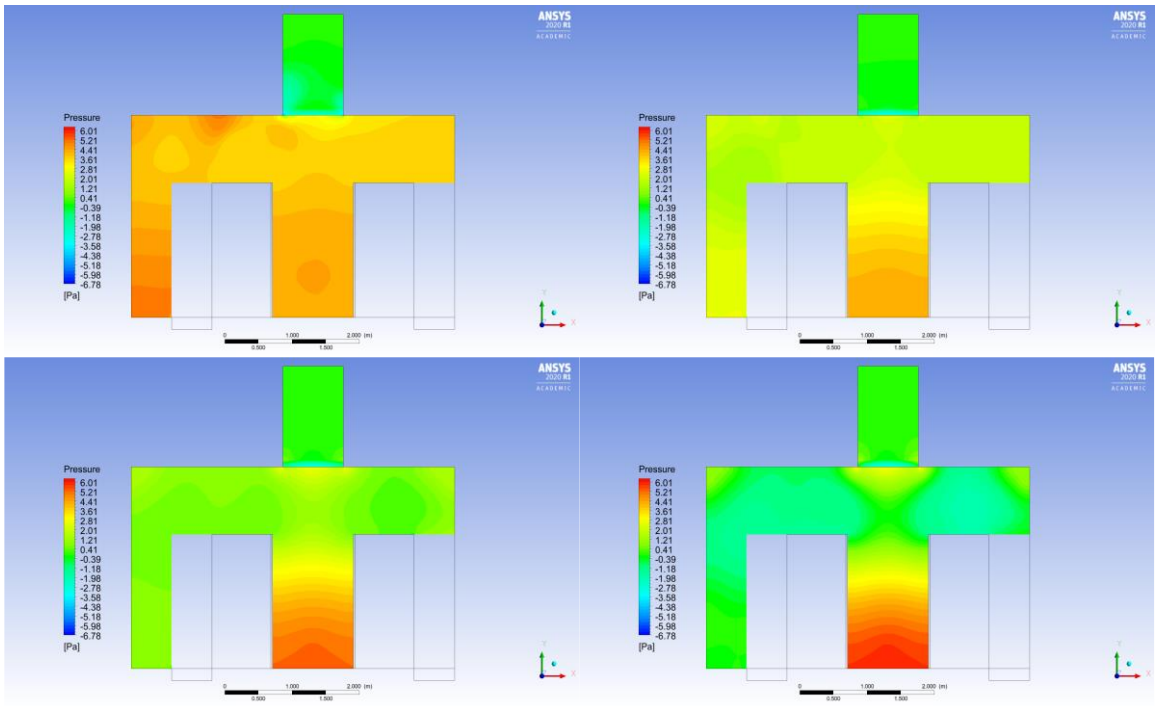

Figure 3-4: 1A (top left), 1B (top right), 1C (bottom left), and 1D (bottom right) Static pressure contours

passes through the rack is obtained directly from the supply which is synonymous with the amount of recirculation being negligible. As the volumetric flow rate ratio increases past unity, there is an increase in the amount of recirculation that occurs. However, there is also an increase in the static pressure gradient in the hot aisle as shown in figure 3-4. Since there is a low-pressure zone above the hot aisle near the return vents, this results in air being forced directly into the return plenum and reduces the mixing with the air adjacent to the hot aisles. However, as is made clear by the changes in the RHI and SHI, the effect of the increased recirculation is greater than the effect of the reduced mixing.

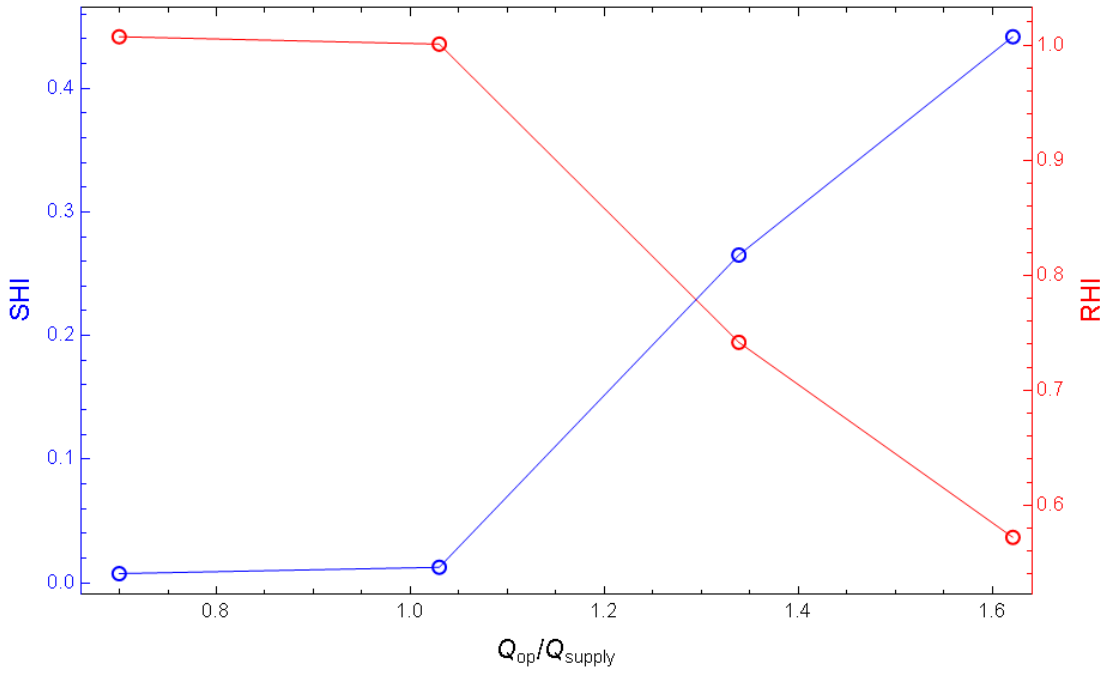

Figure 3-5: Variation of RHI and SHI with volumetric flow rate ratio

Figure 3-6 shows that the RTI increases linearly with respect to the ratio of the operating volumetric flow rate to the supply volumetric flow rate. It is known that the temperature at the rack intakes when there are 2 or 3 fans is equal to the supply temperature, however there is a noticeable difference in the exhaust and return temperatures, resulting in an increase of the RTI by approximately 30%. This can be explained by the fact that for case 1A, a non-negligible amount of the supply air is bypassing the rack entirely which corresponds to a reduction in the mass flow rate through the racks, resulting in higher exhaust and return temperatures. When the volumetric flow rate ratio is greater than unity, it is assumed that the rate at which air is pulled through the through the racks by the fans is greater than the rate at which air is supplied through the underfloor plenum. As a result, surrounding air is pulled in by the racks resulting in hot air from the exhausts to be recirculated back into the intakes. Even though the mass flow rate through the racks has increased, resulting in a higher enthalpy flow rate, due to recirculation the average

intake, exhaust, and return temperatures have increased, the effects of which outweigh that of the increased mass flow rate, ultimately resulting in an increase in the RTI.

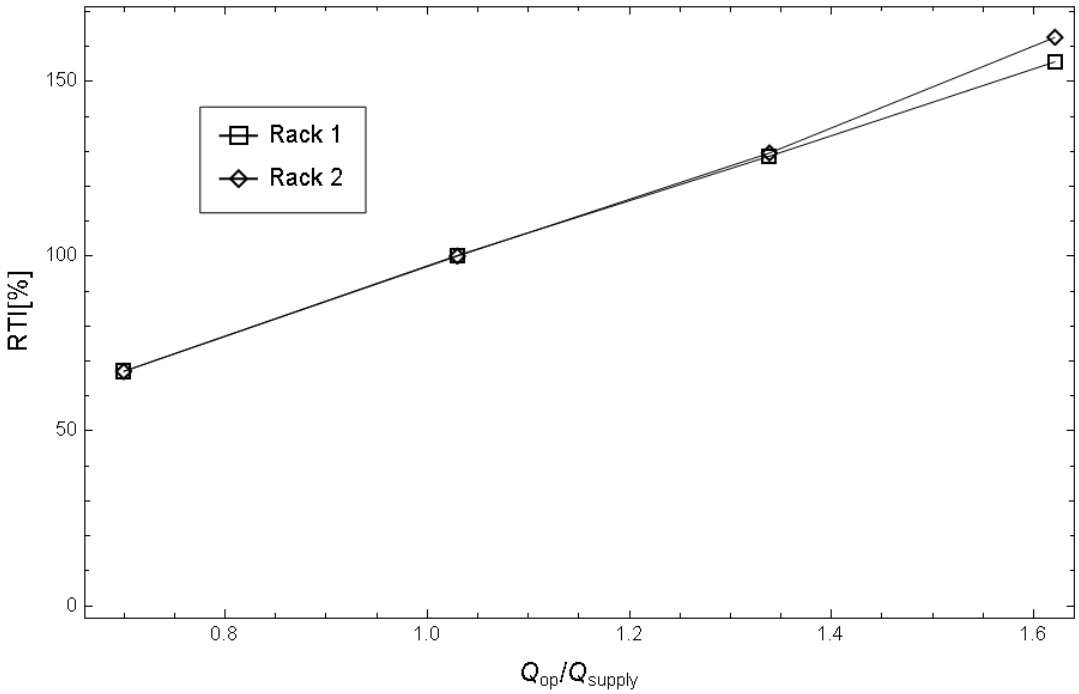

Figure 3-6: Variation of RTI with volumetric flow rate ratio

Such effects on the intake are made clearer by observing the effect of varying the operating volumetric flow rate on the β index. As is clearly seen in figure 3-7, as the volumetric flow rate ratio increases, there is an increase in the maximum intake temperature in addition to the effects of recirculation effecting servers lower on the rack. The variation in the β index is greatest immediately after the volumetric flow ratio becomes greater than unity. This emphasizes the need to select fans that match the volumetric flow rate being supplied to each rack.

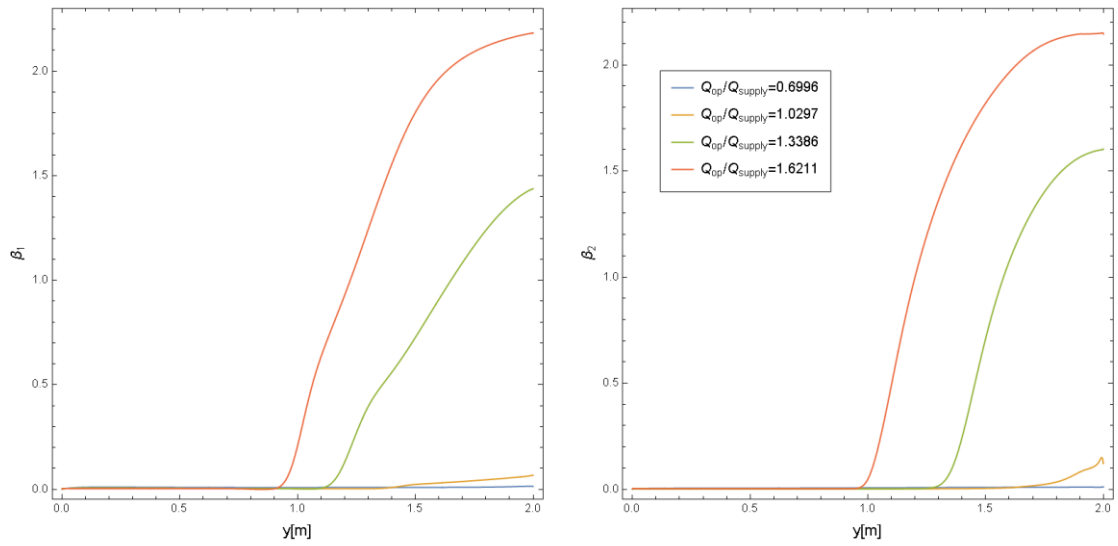

Figure 3-7: Variation of rack 1 (left) and rack 2 (right) β index with operating volumetric flow rate ratio

3.2 Hot Aisle Width

The error of the sum of the SHI and RHI for cases 2A, 2B, and 2C are all under 1.1% as is shown in figure 3-8.

Figure 3-11 illustrates that as the hot aisle width decreases, so too does the SHI, consequently resulting in an increase of the RHI. This is because as the hot aisle width decreases, the static pressure gradient in the hot aisle increases. Since there is a low-pressure zone above the hot aisle, as the static pressure gradient in the hot aisle increases, so too does the velocity at which the air is forced out of the hot aisle. This increased velocity results in a reduction of the mixing of the air in the hot aisle with the air located above the racks. This agrees with the work of Sharma[7] who also observed an increase in the SHI when investigating the effects of hot aisle width using a model of a 3D data center with a ceiling return plenum.

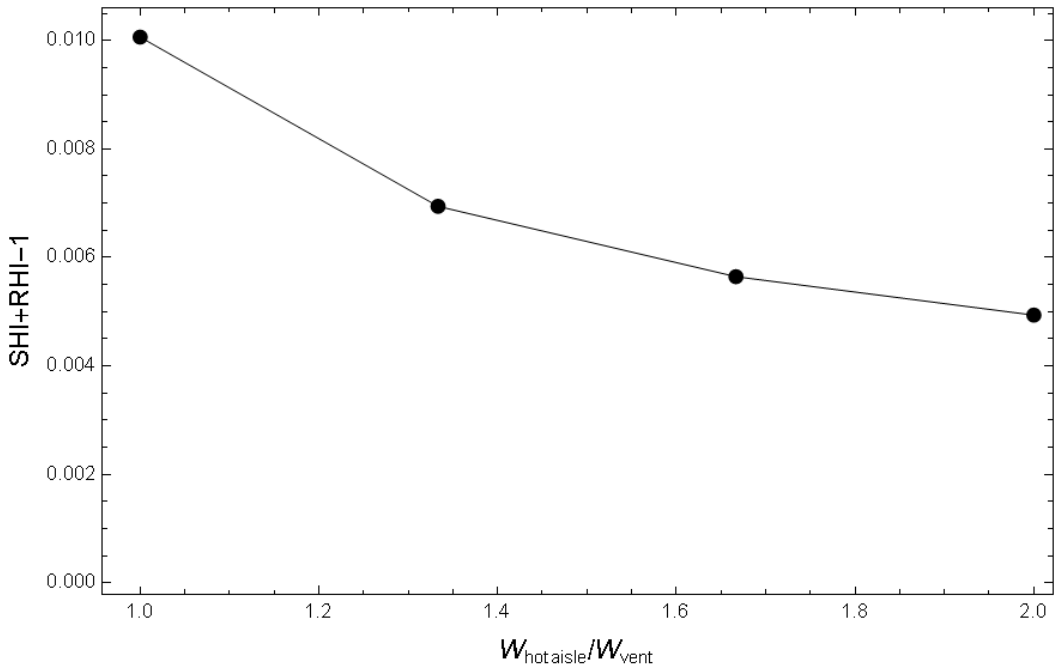

Figure 3-8: Variation of error of sum of SHI and RHI with hot aisle width ratio

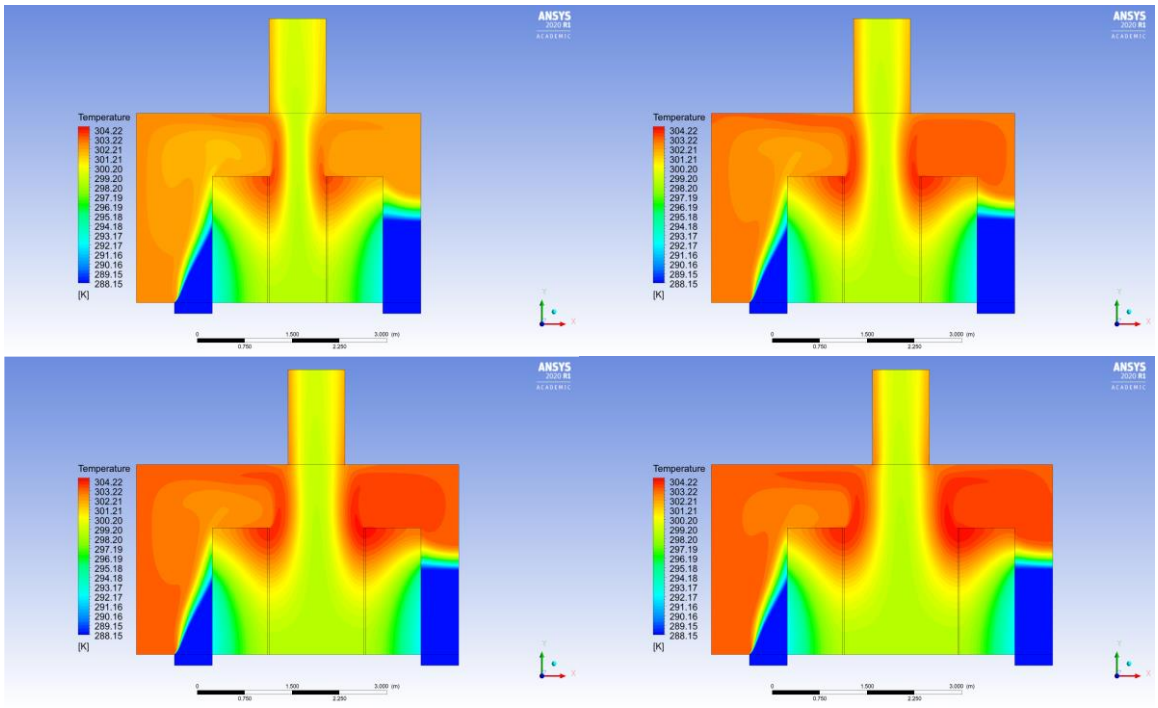

Figure 3-9: 2A (top left), 1C (top right), 2B (bottom left), and 2C (bottom right) temperature contours

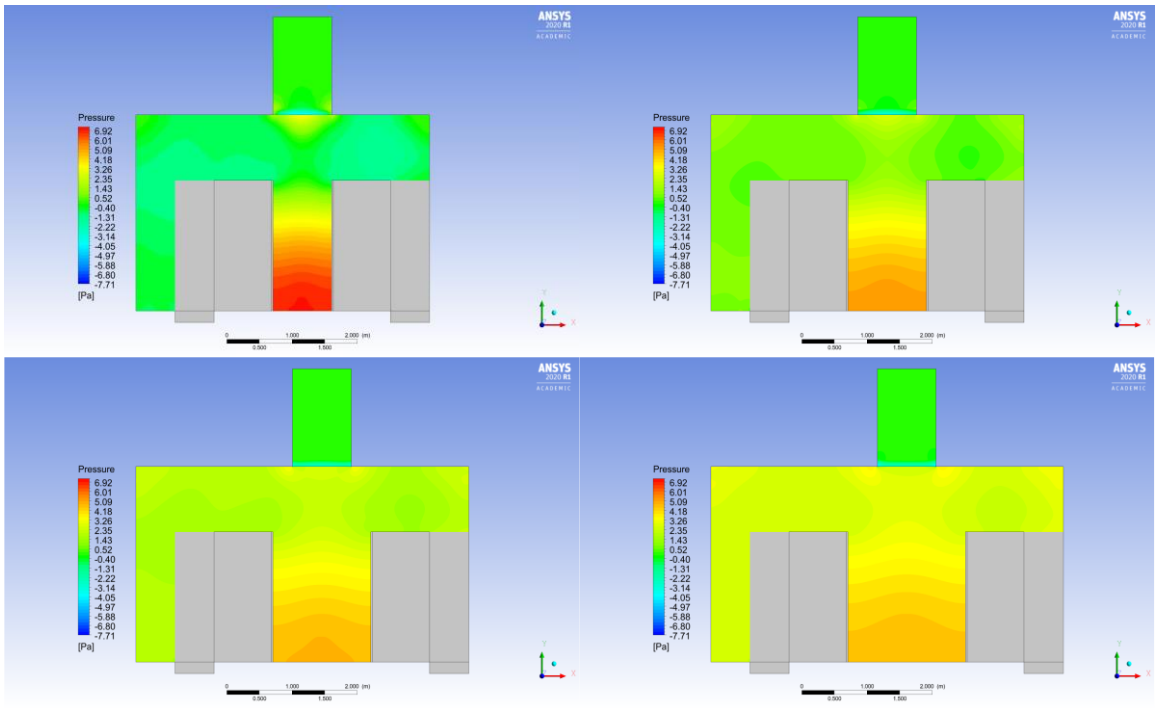

Figure 3-10: 2A (top left), 1C (top right), 2B (bottom left), and 2C (bottom right) static pressure contours

Figure 3-12 shows a decrease in the RTI as the hot aisle width decreases. This is similarly caused by the reduction of the mixing of the hot exhaust air with the air sitting atop the racks. Meanwhile, it is shown in figure 3-13 that as the width decreases, the maximum value of the β index increases and the height at which self-heating occurs, as indicated by the β index being equal to unity, decreases, indicating greater penetration of the heated air into the cold aisles.

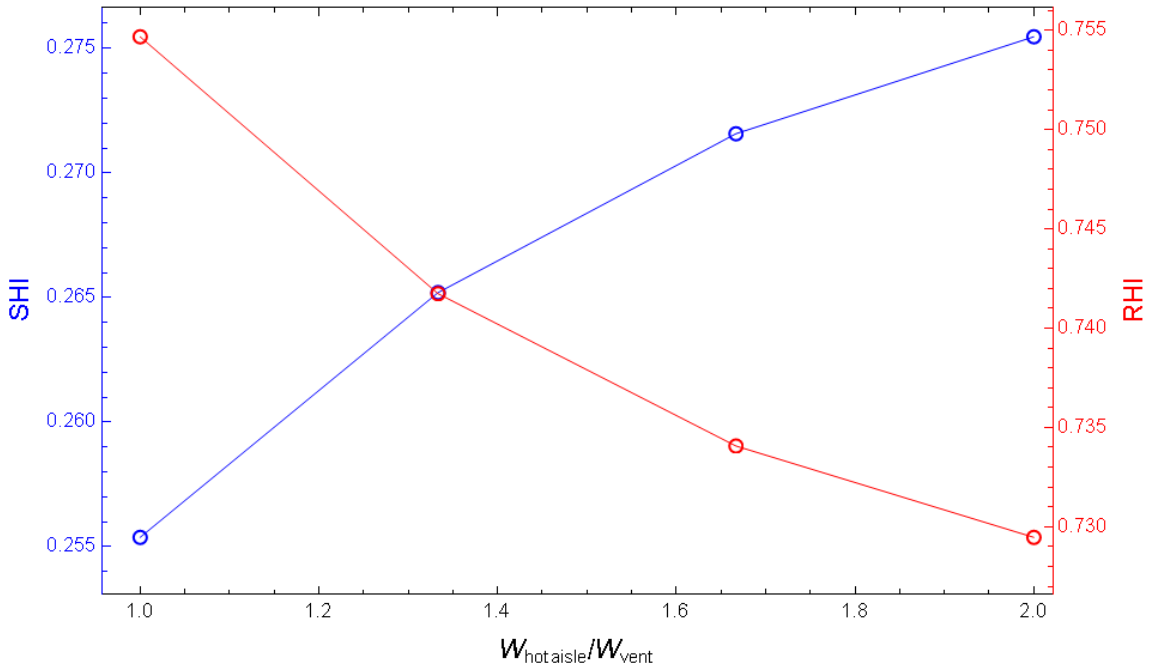

Figure 3-11: Variation of SHI and RHI with hot aisle width ratio

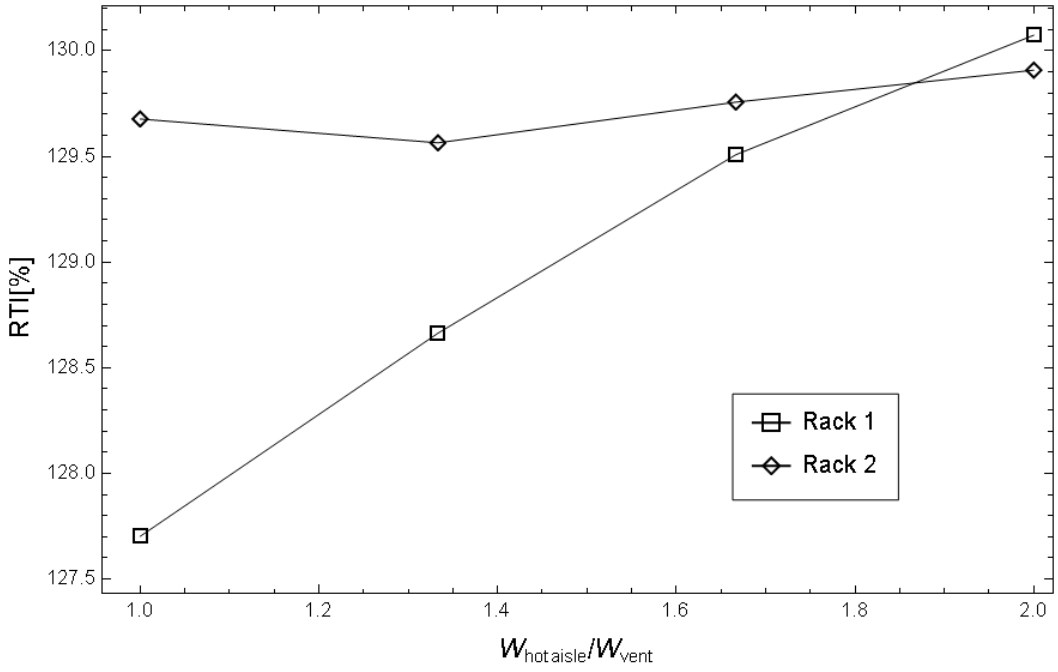

Figure 3-12: Variation of RTI with hot aisle width ratio

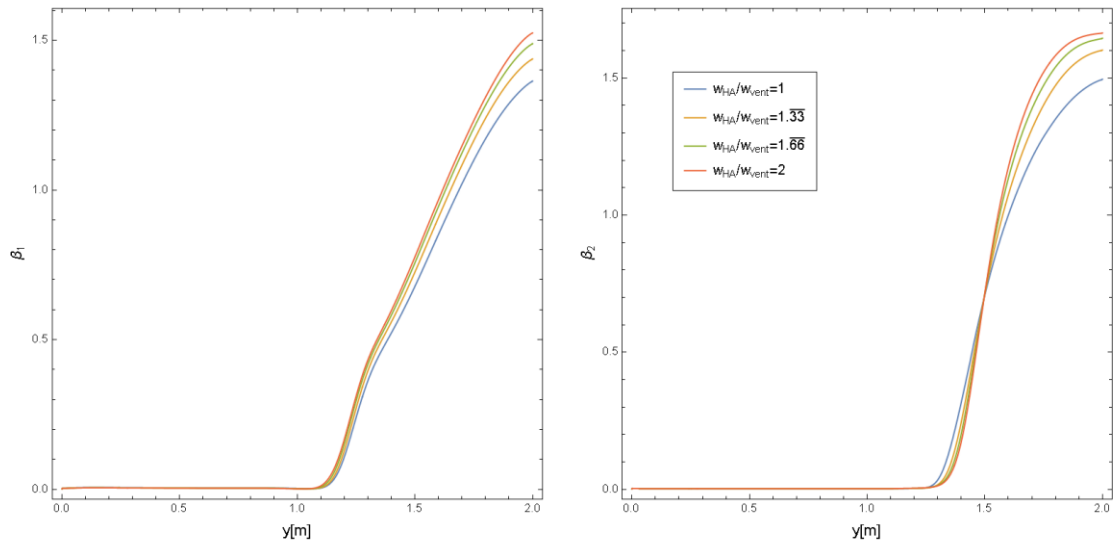

Figure 3-13: Variation of rack 1 (left) and rack 2 (right) β index with hot aisle width ratio

3.3 Ceiling Height

The error of the sum of SHI and RHI for cases 3A, 3B, 3C, and 3D are all under 1% as is shown in figure 3-14.

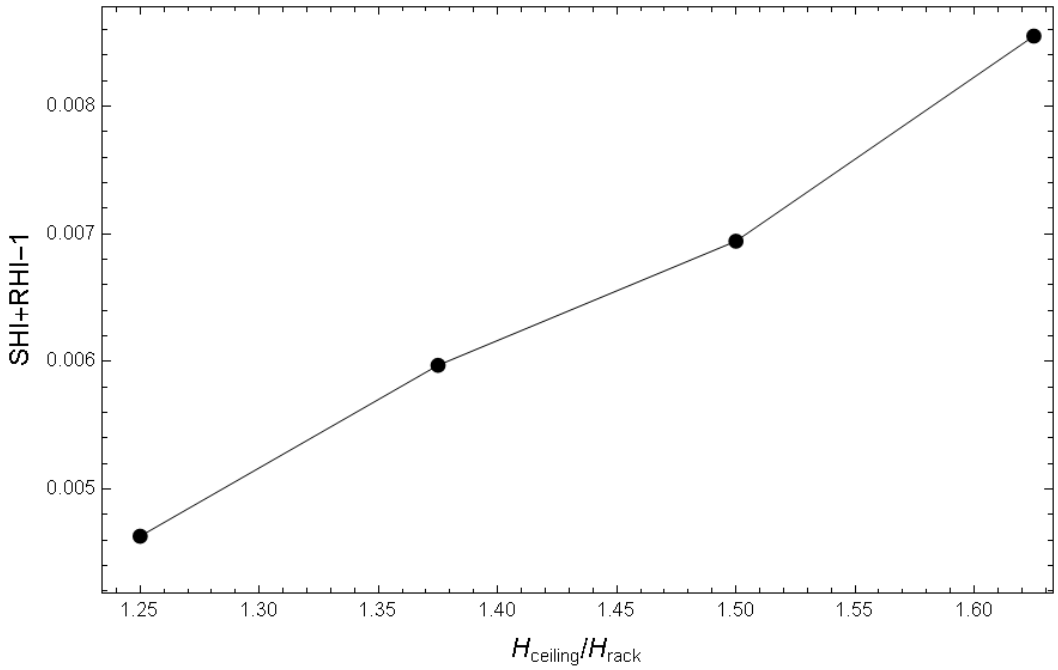

Figure 3-14: Variation of error of sum of SHI and RHI with ceiling height ratio

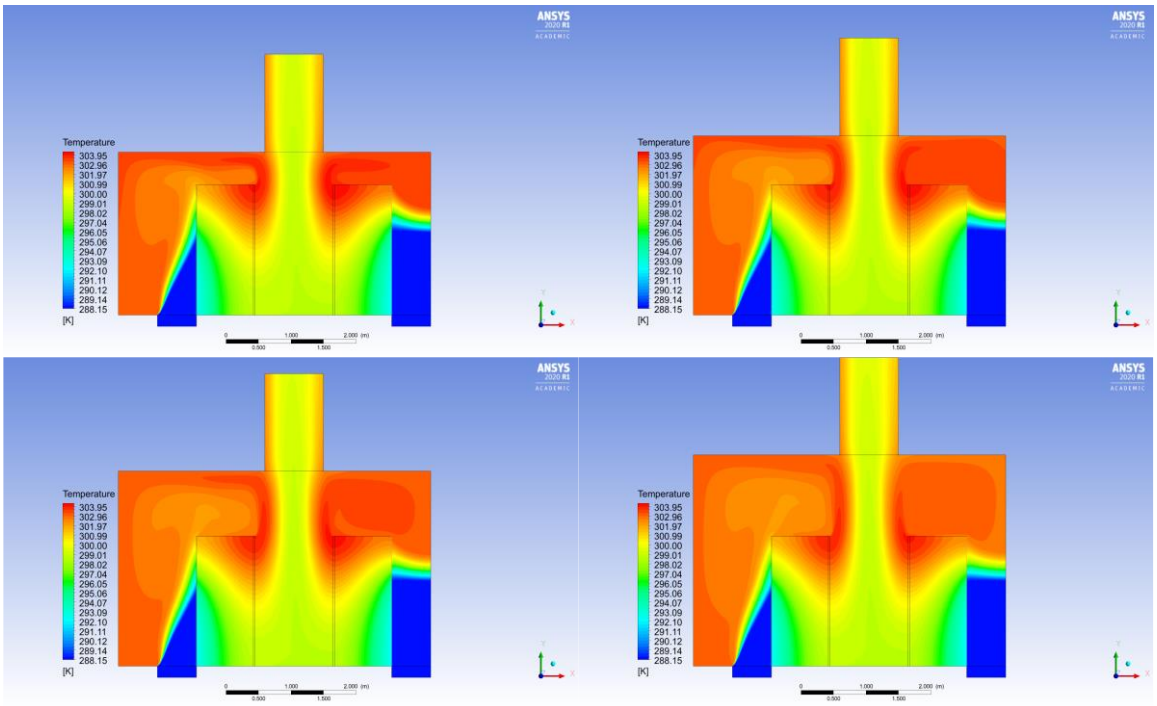

Figure 3-15: 3A (top left), 3B (top right), 1C (bottom left), and 2C (bottom right) temperature contours

Figure 3-16 shows a decrease in the SHI which is indicative of a decrease in the amount of mixing between the hot and cold aisles.

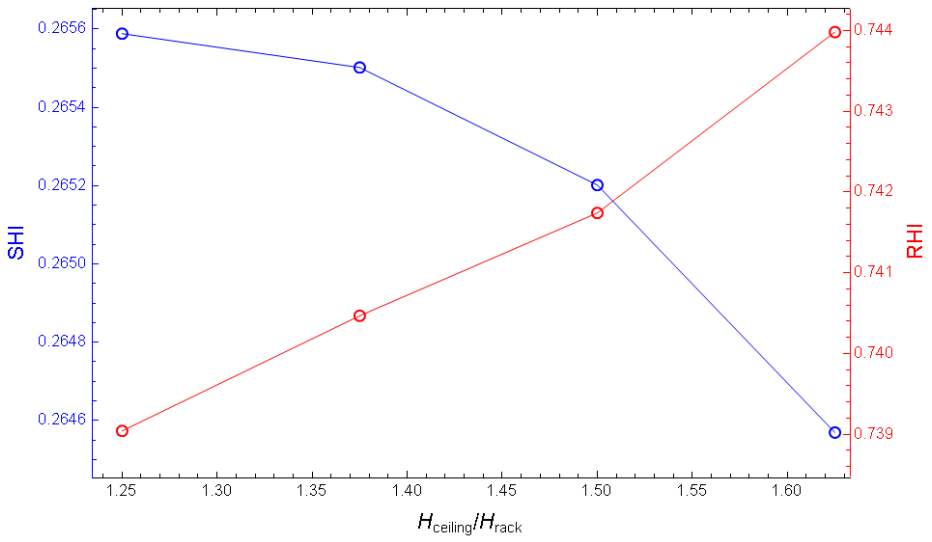

Figure 3-16: Variation of SHI and RHI with ceiling height ratio

The RTI for both the outer and inner racks increase as the ceiling height increases with the effects being much more pronounced for the inner racks while the outer racks show much smaller variations as is illustrated in figure 3-17. This is indicative of an increase in the amount of mixing occurring within the data center. The β index, as shown in figure 3-18, shows a small decrease in the maximum temperature at the intake of the rack and negligible variations of the height at which self-heating occurs.

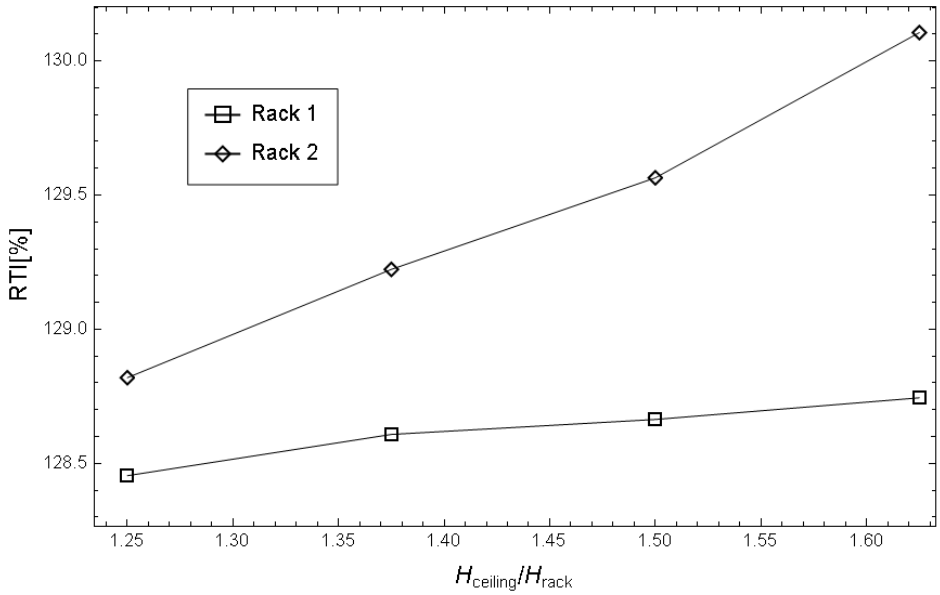

Figure 3-17: Variation of RTI with ceiling height ratio

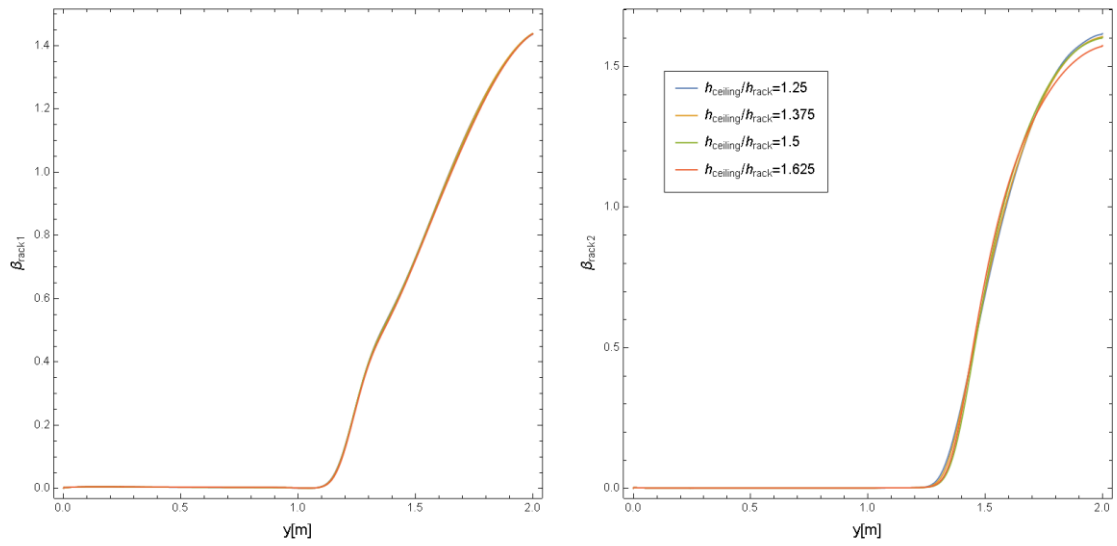

Figure 3-18: Variation of rack 1 (left) and rack 2 (right) β index with ceiling height ratio

3.4 Containment

The purpose of hot aisle containment is to prevent the mixing of the air in the cold and hot aisles. When utilizing hot aisle containment there is no longer an airflow path for recirculation or bypass to occur and all the supply air is forced through the racks. Since all of the air from the supply is forced through the racks, by definition the SHI is zero and the RHI is equal to unity. In addition, it forces all the air from the rack exhaust to the ceiling plenum return which results in an RTI of 100%. Since the flow path is predetermined due to the containment and all the supplied air must travel through the rack in order to leave the system, it is assumed that the effect of containment in the simulation is independent of the of the actual operating volumetric flow rate dictated by the fans. Based on the results of the RTI, SHI, and RHI, which for a hard walled containment system with no leakage must be ideal, one can assume this is a case with optimal cooling efficiency and as such this case is used as a benchmark for comparison with already existing infrastructure with in regards to rack intake, rack exhaust, and room

outlet temperatures. Therefore, the case that uses hot aisle containment shall be compared with the results of case 1B, as this case had index values closest to being optimal.

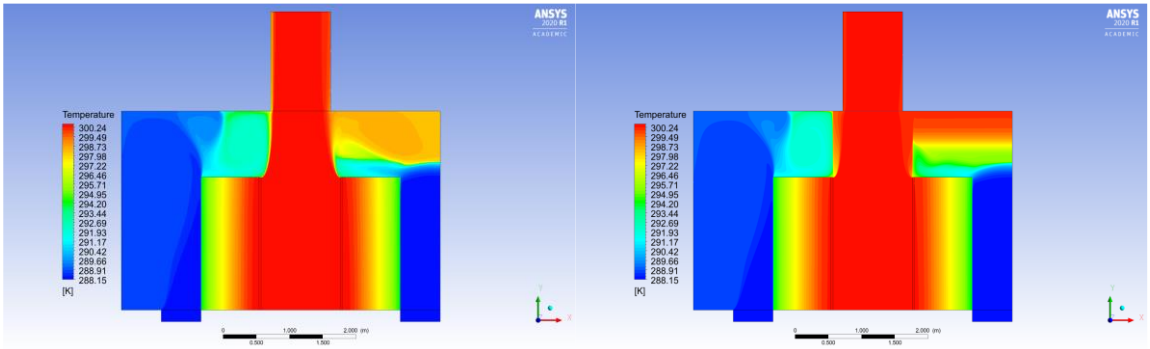

Figure 3-19: 1B (left) and 4A (right) temperature contours

The distinguishable differences observed between the ideal case without containment, and the case with containment, is that the becomes stratified above the cold aisle and inner racks. The average exhaust temperatures for racks 1 and 2 for case 1B are 300.43286K and 300.43182K respectively. For case 4A the average exhaust temperatures are 300.31188K and 300.3041K. This demonstrates that as is seen in figure 3-19 and from the exhaust temperature comparison, a data center can approach the same level of efficiency with or without the use of containment, however, due to the uncertainty of guaranteeing a perfect match of the flow rates through a supply with that of the fans in the servers, the use of containment is comparatively easier as it does not require any guesswork.

CHAPTER 4: CONCLUSION AND FUTURE WORK

This study investigated how varying different design parameters impacts how effectively the server racks in the data center are cooled based upon various thermal metrics such as SHI, RHI, RTI, and β index.

Varying the number of fans determines the ratio of the volumetric flow rate through the racks to the volumetric flow rate through the perforated tile. The volumetric flow rate through the rack can be determined by locating the operating point at the intersection of the fan curve and the system resistance curve. The optimal case is when the volumetric flow rate ratio is equal to 1. When this ratio is less than unity, there is little mixing of hot and cold air in the cold aisle, however, this also increases the amount of air that bypasses the server racks thus resulting in higher exhaust temperatures. When the ratio is greater than unity, there is an increase in the mixing of air from the hot aisles with air from the cold aisles due to an increase in recirculation. As a result of the recirculated air the temperature at the rack intake increases, with the highest temperatures located at the top of the racks. Ideally, one would aim to determine the volumetric flow rate of the supply, and choose fans that will result in a volumetric flow rate through the racks which matches that of the supply while also being able to overcome the pressure losses experienced within the racks.

As the hot aisle width increases, the static pressure in the hot aisle increases. For a ceiling plenum return system this results in the air in the hot aisle being forced upwards out of the hot aisle do to the pressure gradient, accelerating the fluid, and thus reducing the amount of mixing that occurs between the hot aisle and the surrounding fluid. Ideally one would want to make the hot aisle as narrow as possible while leaving enough space for maintenance to be done.

When interpreting the trends shown by the RHI and SHI, the RTI, and the β index caused by variations in the ceiling height, the behavior described by the SHI and RHI are consistent with what is seen in the β index, however, it contradicts the behavior of the

RTI. While the RHI, SHI, and β index all show behavior that is indicative of a decrease in the mixing of the air in the hot aisle with the surrounding fluid, the behavior demonstrated by the RTI is indicative of an increase in mixing. When investigating the variation of SHI and RTI with ceiling height, Sharma had found a relationship that indicated an increase in mixing. Two major differences between the work of Sharma and the current study is the use of a porous media model to represent the server rack and Sharma simulated a data in three dimensions while the current study simulates a data center in two dimensions. Modelling the server rack as a porous media is only an approximation of the server rack and not a geometrically accurate model and a certain level of error is expected, however, the benefit of using such a model is it greatly reduces the computational cost of modelling the servers. Modelling the servers as a porous media has been done in prior studies by Zhang[28], Nada[23], and Fulpagare[29] which lends merit to the accuracy of this methodology. Another possible reason for these contradictory results may be that the presence of mixing in the third dimension has a significant effect on the SHI, RHI, RTI, and β index, and that the phenomena that these indices measure cannot be fully encapsulated using a 2D model. Based on these findings, a later investigation into the differences of results obtained from a data center modelled in 3D rather to the results obtained in 2D, where both models simplified the racks as a porous media with an energy source warrants merit.

Lastly, the use of aisle containment allows for complete control of the flow path that the air takes. It is a simple method to prevent bypass or recirculation and ensures that all the air that is being supplied through the plenum travels through the rack and then immediately is returned to the CRAC. This eliminates the guesswork involved with

trying to match the flow rate through the rack with the flow rate through the supply making it much easier to achieve high levels of cooling efficiency in data centers when compared to attempting to choose the ideal configuring to optimize the cooling system.

REFERENCES

[1] Iyengar, M., Schmidt, R. R., Hamann, H., and VanGilder, J., "Comparison Between Numerical and Experimental Temperature Distributions in a Small Data Center Test Cell," Proc. ASME 2007 InterPACK Conference collocated with the ASME/JSME 2007 Thermal Engineering Heat Transfer Summer Conference, pp. 819-826.
[2] Zhang, X., VanGilder, J. W., Iyengar, M., and Schmidt, R. R., 2008, "Effect of rack modeling detail on the numerical results of a data center test cell," 2008 11th Intersociety Conference on Thermal and Thermomechanical Phenomena in Electronic Systems, IEEE, Orlando, FL, USA
[3] Abdelmaksoud, W. A., Khalifa, H. E., Dang, T. Q., and Elhadidi, B., 2010, "Experimental And Computational Study Of Perforated Floor Tile In Data Centers," 2010 12th IEEE Intersociety Conference on Thermal and Thermomechanical Phenomena in Electronic Systems, IEEE, Las Vegas, NV, USA pp. 1-10.
[4] Arghode, V. K., and Joshi, Y., 2016, Air Flow Management in Raised Floor Data Centers, Springer International Publishing.
[5] Choi, J., Kim, Y., Sivasubramaniam, A., Srebric, J., Wang, Q., and Lee, J., 2008, " A CFD-Based Tool for Studying Temperature in Rack-Mounted Servers," IEEE Transactions on Computers, 57(8), pp. 1129-1142.
[6] Choi, J., Kim, Y., Sivasubramaniam, A., Srebric, J., Wang, Q., and Lee, J., 2007, "Modeling and Managing Thermal Profiles of Rack-mounted Servers with ThermoStat," 2007 IEEE 13th International Symposium on High Performance Computer Architecture, IEEE, Scottsdale, AZ, USA
[7] Sharma, R., Bash, C., and Patel, C., 2002, "Dimensionless Parameters for Evaluation of Thermal Design and Performance of Large-scale Data Centers," 8th AIAA/ASME Joint Thermophysics and Heat Transfer ConferenceSt. Louis, Missouri.
[8] Herrlin, M. K., "Improved data center energy efficiency and thermal performance by advanced airflow analysis," Proc. Digital Power Forum, pp. 10-12.
[9] Herrlin, M. K., "Airflow and Cooling Performance of Data Centers: Two Performance Metrics."
[10] Herrlin, M. K., 2005, "Rack cooling effectiveness in data centers and telecom central offices: The rack cooling index (RCI)," Ashrae Transactions, 111, pp. 725-731.
[11] Schmidt, R. R., Cruz, E. E., and Iyengar, M., 2005, "Challenges of data center thermal management," IBM Journal of Research and Development, 49(4.5), pp. 709-723.
[12] "Realizable k-ϵ Model," https://www.afs.enea.it/project/neptunius/docs/fluent/html/th/node60.htm.
[13] "Heat Transfer Theory," https://www.afs.enea.it/project/neptunius/docs/fluent/html/th/node107.htm#sec-hxfer-theory-viscous.
[14] Davis, G. D. V., 1983, "Natural convection of air in a square cavity: A bench mark numerical solution," International Journal for Numerical Methods in Fluids, 3(3), pp. 249-264.
[15] Manzari, M. T., 1999, "An Explicit Finite Element Algorithm for Convection Heat Transfer Problems," International Journal of Numerical Methods for Heat & Fluid Flow, 9(8), pp. 860-877.

[16] Mayne, D. A., Usmani, A., and Crapper, M., 2000, "h-Adaptive Finite Element Solution of High Rayleigh Number Thermally Driven Cavity Problem," International Journal of Numerical Methods for Heat & Fluid Flow, 10, pp. 598-615.
[17] Wan, D. C., Patnaik, B. S. V., and Wei, G. W., 2001, "A NEW BENCHMARK QUALITY SOLUTION FOR THE BUOYANCY-DRIVEN CAVITY BY DISCRETE SINGULAR CONVOLUTION," Numerical Heat Transfer, Part B: Fundamentals, 40(3), pp. 199-228.
[18] Ramaswamy, B., Jue, T. C., and Akin, J. E., 1992, "Semi-implicit and Explicit Finite Element Schemes for Coupled Fluid/Thermal Problems," International Journal for Numerical Methods in Engineering, 34(2), pp. 675-696.
[19] Massarotti, N., Nithiarasu, P., and Zienkiewicz, O. C., 1998, "Characteristic Based Split (CBS) Algorithm for Incompressible Flow Problems with Heat Transfer," International Journal of Numerical Methods for Heat & Fluid Flow, 8, pp. 969-990.
[20] Benedict, R. P., 1980, Fundamentals of pipe flow, Wiley, New York.
[21] Holle, G. F., 1986, "Evaluation and Analysis of Gas Turbine Internal Flow Restrictors," UNIVERSAL ENERGY SYSTEMS INC DAYTON OH.
[22] Idel'chik, I. E., and Steinberg, M. O., 1994, Handbook of hydraulic resistance, CRC Press, Boca Raton, FL.
[23] Nada, S. A., Said, M. A., and Rady, M. A., 2016, "CFD investigations of data centers thermal performance for different configurations of CRACs units and aisles separation," Alexandria Engineering Journal, 55(2), pp. 959-971.
[24] 2020, "ANSYS Fluent Theory Guide," ANSYS, Inc.
[25] Pandiyan, V., 2012, "Development of Detailed Computational Flow Model of High End Server and Validation Using Experimental Methods," Master of Science in Mechanical Engineering Masters Thesis, The University of Texas at Arlington.
[26] Furuta, S., 2011, "Server Chassis and Triplet Hardware v1.0," Facebook, Inc.
[27] Nagendran, B., 2013, "Improving Cooling Efficiency Of Servers By Replacing Smaller Chassis Enclosed Fans With Larger Rack-Mount Fans," Master of Science in Mechanical Engineering, The University of Texas at Arlington.
[28] Zhang, J., 2012, "Cooling of electronic system."
[29] Fulpagare, Y., Joshi, Y., and Bhargav, A., "Transient Characterization of Data Center Racks," Proc. ASME 2016 International Mechanical Engineering Congress and ExpositionV008T10A007.